JAMES | Journal of Advances in Modeling Earth Systems

RESEARCH ARTICLE
10.1029/2024MS004482

Key Points:

- A computationally-efficient sensitivity analysis identifies key parameters and physical mechanisms for global climate properties
- Certain parameter sensitivities in short-term, initialized hindcasts are consistent with those seen in multidecadal climate simulations
- Parameters governing the degree of turbulent mixing in the presence of vertical wind shear are influential for surface stress representation

Supporting Information:

Supporting Information may be found in the online version of this article.

Correspondence to:

K. M. Nardi,
kmn182@psu.edu

Citation:

Nardi, K. M., Zarzycki, C. M., & Larson, V. E. (2024). A method for interpreting the role of parameterized turbulence on global metrics in the Community Earth System Model. *Journal of Advances in Modeling Earth Systems*, *16*, e2024MS004482. https://doi.org/10.1029/2024MS004482

Received 5 JUN 2024
Accepted 6 OCT 2024

A Method for Interpreting the Role of Parameterized Turbulence on Global Metrics in the Community Earth System Model

Kyle M. Nardi[1], Colin M. Zarzycki[1], and Vincent E. Larson[2,3]

[1]Department of Meteorology and Atmospheric Science, The Pennsylvania State University, University Park, PA, USA, [2]Department of Mathematical Sciences, University of Wisconsin-Milwaukee, Milwaukee, WI, USA, [3]Pacific Northwest National Laboratory, Richland, WA, USA

Abstract The parameterization of subgrid-scale processes such as boundary layer (PBL) turbulence introduces uncertainty in Earth System Model (ESM) results. This uncertainty can contribute to or exacerbate existing biases in representing key physical processes. This study analyzes the influence of tunable parameters in an experimental version of the Cloud Layers Unified by Binormals (CLUBBX) scheme. CLUBB is the operational PBL parameterization in the Community Atmosphere Model version 6 (CAM6), the atmospheric component of the Community ESM version 2 (CESM2). We perform the Morris one-at-a-time (MOAT) parameter sensitivity analysis using short-term (3-day), initialized hindcasts of CAM6-CLUBBX with 24 unique initial conditions. Several input parameters modulating vertical momentum flux appear most influential for various regionally-averaged quantities, namely surface stress and shortwave cloud forcing (SWCF). These parameter sensitivities have a spatial dependence, with parameters governing momentum flux most influential in regions of high vertical wind shear (e.g., the mid-latitude storm tracks). We next evaluate several experimental 20-year simulations of CAM6-CLUBBX with targeted parameter perturbations. We find that parameter perturbations produce similar physical mechanisms in both short-term and long-term simulations, but these physical responses can be muted due to nonlinear feedbacks manifesting over time scales longer than 3 days, thus causing differences in how output metrics respond in the long-term simulations. Analysis of turbulent fluxes in CLUBBX indicates that the influential parameters affect vertical fluxes of heat, moisture, and momentum, providing physical pathways for the sensitivities identified in this study.

Plain Language Summary Models struggle with certain aspects of predicting the Earth's current and future climate. To achieve better predictions in the future, it is important to understand which parts of the model need to be improved. This study explores how changing certain model characteristics influences what the model outputs. We find that changing how the model estimates small-scale motions in the atmosphere improves the model's accuracy. Furthermore, these changes affect both short-term (several days) and long-term (several decades) model simulations. The results of this study can help scientists understand the physical behavior of climate models and help inform future improvements to enhance model accuracy.

1. Introduction

Despite continued advances in computational capacity, Earth System Models (ESMs) still exhibit notable biases in depicting key processes relevant to the climate system. These include cloud-radiative forcings (e.g., Trenberth & Fasullo, 2010) and surface wind stress (e.g., Simpson et al., 2018), just two examples of processes critical for accurately depicting the future climate in an ESM. Generally, ESMs do not explicitly resolve processes related to clouds, radiation, convection, microphysics, and boundary layer (PBL) turbulence, even at grid spacings considered high-resolution for climate applications (Bacmeister et al., 2014, 2018; Wehner et al., 2014). Therefore, ESMs must estimate, or parameterize, these key physical processes based on theory, observations, or a combination of both. These parameterizations typically contain tunable numeric settings (i.e., parameter values) and are a key source of uncertainty in ESMs (e.g., Covey et al., 2013; Duffy et al., 2024; Nardi et al., 2022; Qian et al., 2018).

Parameterizations are a major source of model uncertainty because (a) parameter values are often inadequately constrained physically due to a lack of process-level understanding or observational data and (b) there are often various ways model developers can represent the same process (Hourdin et al., 2017). Recent studies have

focused on better quantifying uncertainties in ESM output due to choice of parameter value. Many of these studies have performed variations of a perturbed parameter ensemble (PPE), in which a model is run multiple times with unique combinations of input parameter values. The changes in model outputs across different parameter combinations help quantify the degree to which each input parameter affects the model solution. For example, Eidhammer et al. (2024) performed a PPE in which they used Latin hypercube sampling to perturb 45 input parameters associated with the PBL turbulence, microphysics, and convection parameterization schemes in the Community ESM version 2 (CESM2). This PPE guided the identification of key parameters for more focused perturbations and analysis (Duffy et al., 2024).

Qian et al. (2018) performed a PPE on 18 parameters from the turbulence/shallow convection, microphysics, deep convection, and gravity wave drag schemes in the Energy Exascale Earth System Model (E3SM). Unlike the PPE in Eidhammer et al. (2024), they ran short, 3-day simulations rather than multiyear simulations. Such a methodology provides the added benefit of reduced computational cost and better ability to sample a larger parameter space. This study demonstrated that short-term simulations can provide useful insights for parameter sensitivity at longer time scales. These are just several examples among numerous other parameter sensitivity analyses using ESMs (e.g., Covey et al., 2013; Guo et al., 2014, 2015; Ma et al., 2014; Qian et al., 2015).

Though previous work has highlighted influential parameters for ESMs, the precise physical mechanisms driving these parameter sensitivities remain uncertain. Recent studies have attempted to fill this gap in model development. For example, prior studies have found that parameters affecting the subgrid-scale distribution of vertical velocity play a key role in modeled cloud regimes (e.g., Guo et al., 2015; Qian et al., 2018). Graap and Zarzycki (2024) analyzed how changes in the formulation of momentum flux in CESM2 affected low-level fluxes of momentum, heat, and moisture in the tropical Atlantic. They found that adding a prognostic formulation for vertical momentum flux in the PBL turbulence scheme improved the depiction of modeled fluxes, producing more realistic low-level wind profiles. Nardi et al. (2022) conducted a one-at-a-time sensitivity analysis and identified a handful of input parameters related to PBL turbulence that were influential in the depiction of PBL structure in idealized tropical cyclones (TCs) in CESM2. They linked the influential input parameters to the modulation of turbulent eddy length scales and vertical turbulent mixing in the TC PBL.

While Nardi et al. (2022) established the importance of parameterized momentum flux on TC structure in CESM2, it is unclear how these parameters affect output in a more realistic global simulation. In particular, we wish to better understand how and *why* these parameters influence various aspects of the climate system. As in Nardi et al. (2022), we seek to screen a larger number of input parameters to isolate a handful of parameters that are influential for the mean climate. We can then isolate these parameters and analyze the physical drivers behind the sensitivities. Knowledge of PBL parameters that affect the global climate system, and those that affect extreme weather phenomena, can inform model developers when balancing improvements aimed at either objective. We also seek a screening mechanism that reduces computational cost while also allowing for a comprehensive analysis of parameter sensitivity in the climate system.

In this study, we employ a simple parameter sensitivity analysis, Morris one-at-a-time or MOAT (Morris, 1991), on a subset of tunable input parameters in the PBL turbulence and microphysics schemes within an ESM. Following prior ESM sensitivity analyses, we first focus on a handful of spatiotemporally-averaged output metrics related to cloud-radiative forcing. We then compare parameter sensitivities for common parameters between studies to verify the fidelity of our MOAT analysis (Section 3.1). We then build on prior studies and extend our analysis to less commonly-evaluated metrics related to PBL turbulence, the general circulation, and precipitation processes (Section 3.2). We next evaluate the key physical mechanisms driving the influence of one particular influential input parameter (Section 3.3). We conclude by running a 20-year CESM2 simulation with two targeted parameter perturbations, informed by the short-term MOAT sensitivity analysis (Section 3.4).

This study builds on prior PPEs in three ways. First, we extend our analysis beyond cloud-radiative metrics and analyze metrics characterizing the PBL and general circulation. This allows a more comprehensive view of how tunable parameters affect all components of the climate system. Second, we explore a handful of experimental input parameters in the PBL turbulence parameterization that have not been thoroughly studied in prior PPEs. Third, we analyze process-oriented metrics to help identify physical mechanisms driving parameter sensitivities. While short-term simulations isolate relevant physical mechanisms prior to the onset of feedbacks manifesting at longer time scales, multi-year simulations allow for a deeper analysis of how parameter perturbations affect

interactions within the modeled climate system (e.g., turbulence, clouds, microphysics). In this way, our analysis will not only guide model tuning but also provide key context that can allow model developers to build a more physically-consistent model.

2. Materials and Methods

2.1. Model Setup

We evaluate input parameter sensitivity in the Community Atmosphere Model version 6 (CAM6), the atmospheric component of CESM2 (Danabasoglu et al., 2020). We run CAM6 using the spectral element (SE) dynamical core (Dennis et al., 2012; Lauritzen et al., 2018) on a 1°cubed-sphere grid with a hybrid sigma-pressure vertical coordinate (58 levels). The development version of CAM6 used here is tagged *cam6_3_124* (https://github.com/ESCOMP/CAM/releases/tag/cam6_3_124). Notably, this version of CAM6 employs the Parameterization of Unified Microphysics Across Scales version 1 (PUMASv1; Gettelman et al., 2023) scheme to parameterize microphysics and an experimental version of the Cloud Layers Unified by Binormals (CLUBB; Golaz et al., 2002; Larson, 2017; Larson et al., 2019) scheme to parameterize PBL turbulence, shallow convection, and cloud macrophysics.

We initialize CAM6 with atmospheric states, sea-surface temperatures (SST), and sea ice conditions from reanalysis and integrate over 72 hr ("Betacast," C. Zarzycki, 2023). We initialize the atmosphere from the 5^{th} generation of the European Center for Medium-Range Weather Forecasts (ECMWF) reanalysis (ERA5; Hersbach et al., 2017). We initialize SST and sea ice with daily data from the NOAA Optimum Interpolation version 2 data set (NOAA OI SST v2; Reynolds et al., 2002). Both ERA5 and NOAA OI SST v2 data are at a horizontal resolution of 0.25°. To initialize the land, we follow Pettett and Zarzycki (2023) and apply a 12-month spin-up process in which we run the Community Land Model version 5 (CLM5; Lawrence et al., 2019) with prescribed atmospheric conditions from ERA5 over the 12 months preceding the initialization date. SST and sea ice remain constant throughout the entirety of the short model run. To encompass seasonal variations and account for interannual variability, we run Betacast for 24 different initialization dates. For each month (January-December), we randomly select two years between 2010 and 2020, and for each month-year combination, we initialize the model at 00 UTC on the first day of the month. While randomly sampled initially, we keep these initializations fixed for each parameter combination.

Though prior sensitivity analyses have leveraged multi-year simulations in ESMs (e.g., Eidhammer et al., 2024; Guo et al., 2015; Zhang et al., 2018), we choose to use 3-day hindcasts for three reasons: (a) running short simulations reduces computational cost, thus allowing for an expanded sampling of the parameter space, (b) short simulations allow for the isolation of key physical processes before nonlinear feedbacks manifest, and (c) short simulations have proven effective in understanding parameter sensitivity in multi-year ESM simulations (Ma et al., 2014; Qian et al., 2018; Wan et al., 2014; Xie et al., 2012). Qian et al. (2018) specifically demonstrated that short simulations are useful tools for establishing a process-level understanding of a parameterization's influence on "fast processes" involving clouds, convection, and turbulence. They showed that parameter sensitivities seen in 3-day E3SM simulations are comparable to those in 5-year simulations.

2.2. Cloud Layers Unified by Binormals (CLUBB)

CLUBB is a unified parameterization for turbulence, shallow convection, and cloud macrophysics in CAM6 (Golaz et al., 2002). The governing equations for CLUBB are detailed in Larson (2017). Following Nardi et al. (2022), we adopt two experimental modifications to CLUBB. Hereafter, we refer to this version of CLUBB, described below, as CLUBBX.

First, we replace the existing diagnostic formulation of vertical momentum flux, $\overline{u'w'} = -K_m \frac{\partial \overline{u}}{\partial z}$, with a new prognostic formulation, as described in Larson et al. (2019). They noted that the prognostic momentum flux formulation better accounts for upgradient fluxes seen in large eddy simulations. Graap and Zarzycki (2024) demonstrated that implementing the prognostic formulation in CAM6 effectively produced upgradient fluxes over the tropics. However, a detailed analysis of upgradient fluxes is beyond the scope of this study. The prognostic formulation is defined as follows:

$$\frac{\partial \overline{u'w'}}{\partial t} = \underbrace{-\overline{w}\frac{\partial \overline{u'w'}}{\partial z}}_{1} \underbrace{-\frac{1}{\rho}\frac{\partial \rho \overline{w'^2 u'}}{\partial z}}_{2} \underbrace{-(1-C_{uu,shr})\overline{w'^2}\frac{\partial \overline{u}}{\partial z}}_{3} \underbrace{-(1-C_7)\overline{u'w'}\frac{\partial \overline{w}}{\partial z}}_{4} + \underbrace{(1-C_7)\frac{g}{\theta_{vs}}\overline{u'\theta_v'}}_{5} \underbrace{-\frac{C_6}{\tau}\overline{u'w'}}_{6} \underbrace{-\epsilon_{uw}}_{7}. \quad (1)$$

The time tendency equation for $\overline{v'w'}$ is the same but replaces u with v. Here, the mean refers to the average over the grid cell, and the perturbation is the deviation from the grid cell average. ρ represents the air density $\left(\frac{kg}{m^3}\right)$, g represents gravitational acceleration $\left(\frac{m}{s^2}\right)$, θ_v represents the virtual potential temperature (K), and θ_{vs} represents the basic state virtual potential temperature (K). For details about the physical interpretation of each term, refer to Larson et al. (2019).

Second, we employ an experimental formulation for the vertical turbulent eddy length scale L (Guo et al., 2021). This updated formulation diagnoses L using the inverse of the turbulent eddy turnover time scale τ. The inverse $\frac{1}{\tau}$ is a measure of the dissipation of turbulent eddies and is the sum of several eddy-dissipating processes, including near-surface friction, wind shear, and stable stratification:

$$\frac{1}{\tau} = \underbrace{C_{bkgnd}\frac{1}{\alpha}}_{1} + \underbrace{C_{sfc}\frac{u^*}{\kappa}\frac{1}{(z - z_{sfc} + z_{displace})}}_{2} + \underbrace{C_{shear}\sqrt{\left(\frac{\partial \overline{u}}{\partial z}\right)^2 + \left(\frac{\partial \overline{v}}{\partial z}\right)^2}}_{3} + \underbrace{C_{N2}\sqrt{N^2}}_{4} \quad (2)$$

where $\alpha = 1000$ s is a constant (representing artificial background dissipation), u^* is the friction velocity $\left(\frac{m}{s}\right)$, z is height (m), z_{sfc} is surface height (m), $z_{displace}$ is a small $O(10\text{ m})$, constant displacement height introduced to avoid a singularity at the lower boundary (Guo et al., 2021), and N^2 is the square of the Brunt-Väisälä frequency $\left(\frac{1}{s^2}\right)$. Each term on the r.h.s. has a tunable coefficient C_{xxx} that modulates the impact of each eddy-dissipating process.

2.3. Morris One-at-a-Time (MOAT) Method

The Morris One-at-a-Time (MOAT) sensitivity analysis (Campolongo et al., 2007; Morris, 1991) is a computationally-efficient method of screening a large number of input parameters and identifying those that are relatively influential. Parameter values are perturbed one-at-a-time with all other parameter values remaining constant. MOAT quantifies the magnitude, direction, and nonlinearity of the modeled response to perturbing each input parameter individually. The MOAT method has been applied to sensitivity analyses for high-resolution numerical weather models (e.g., Chinta et al., 2021; Morales et al., 2019), single-column models (e.g., Smalley et al., 2022; Suselj et al., 2020) and ESMs (e.g., Covey et al., 2013; Nardi et al., 2022; Pathak et al., 2020). Despite some noted drawbacks, namely incomplete sampling of the parameter space and limited information about nonlinear effects (Morales et al., 2019), the MOAT method provides an effective, computationally-efficient alternative to other sensitivity analyses (e.g., J. D. Herman et al., 2013).

We perturb 17 input parameters, as described in Table 1. Here, "input parameter" is synonymous with terms such as "model tuning coefficient" or "parameterization calibration setting." 13 are CLUBBX parameters tied to the simulation of momentum and scalar fluxes in CLUBBX. We also choose to explore four microphysics parameters that have been included in a prior CAM6 PPE (Eidhammer et al., 2024), allowing us to use the sensitivity of these parameters as a point of comparison between studies. Several of the CLUBBX parameters are experimental coefficients in the formulation of prognostic momentum flux (*c_uu_xxx*) and eddy dissipation (*C_invrs_tau_xxx*). We choose existing CLUBBX parameters due to their importance in modulating ESM output, namely clouds (e.g., Guo et al., 2014; Guo et al., 2015; Qian et al., 2018; Zhang et al., 2018). We choose microphysics parameters based on their demonstrated influence on cloud forcings in CAM6 (Eidhammer et al., 2024). We construct perturbation ranges for the 17 parameters (Table 1) based on precedent from prior studies, consultation with CLUBBX developers, and numerical stability experiments (not shown).

MOAT starts with an initial combination of 17 input parameter values, each randomly selected from a uniform, evenly-spaced distribution of four values spanning the parameter's perturbation range. A new combination of

Table 1
Input Parameters Analyzed in MOAT Sensitivity Analysis

Parameter	Description	Perturbed range
C_invrs_tau_sfc (C_{sfc})	Coefficient in near-surface term in CLUBBX formulation of eddy dissipation	0.05–0.2
C_invrs_tau_shear (C_{shear})	Coefficient in shear term in CLUBBX formulation of eddy dissipation	0.16–0.4
C_invrs_tau_N2 (C_{N2})	Coefficient in static stability term in CLUBBX formulation of eddy dissipation	0.16–0.4
C_invrs_tau_N2_xp2	Coefficient in static stability term in CLUBBX formulation of eddy dissipation (applies to scalar fluxes only)	0–0.8
C_invrs_tau_N2_wp2	Coefficient in static stability term in CLUBBX formulation of eddy dissipation (applies to $\overline{w'^2}$ only)	0.1–1.1
gamma_coef	Controls width of vertical velocity of each Gaussian component	0.1–0.6
gamma_coefb	Controls width of the Gaussian for vertical velocity	0.1–0.6
clubb_C11	Low-buoyancy damping coefficient for vertical velocity skewness	0.2–0.8
clubb_C8	Newtonian damping coefficient for vertical velocity skewness	0.7–5
clubb_beta	Coefficient in the skewness of scalar quantities	1.2–2.6
c_uu_shr ($C_{uu,shr}$)	Coefficient in a pressure term that damps turbulent production of momentum flux and accumulation term for vertical velocity variance	0.01–0.99
c_uu_buoy	Coefficient in a pressure term that damps buoyant production of vertical velocity variance	0–0.99
clubb_up2_sfc_coef	Coefficient multiplied by the friction velocity to calculate surface horizontal wind variances	1–5
micro_mg_dcs	Size threshold for the autoconversion of cloud ice particles to snow	3×10^{-4}–7×10^{-4}
micro_mg_vtrmi_factor	Multiplicative factor for calculating the ice fall velocity	0.5–5
micro_mg_pre_fact	Multiplicative factor for calculating evaporation of precipitation	0.1–1.5
micro_mg_accre_enhan_fact	Enhancement factor for calculating accretion	0.5–5

Note. Parameters 1 through 13 appear in the PBL turbulence scheme (CLUBBX), while parameters 14 through 17 appear in the microphysics scheme (PUMASv1). For parameters that appear in equations herein, we also provide in parentheses the coefficients as they are shown in those equations. Note that these parameters are unitless.

input parameters is generated by perturbing one input parameter value and keeping all other values constant. New combinations are subsequently generated until all 17 input parameters have been perturbed once. This is repeated for additional "paths," each with unique initial combinations of randomly-defined input parameter values. We generate parameter combinations over $M = 10$ paths (Morales et al., 2019), resulting in 180 unique combinations of input parameter values. This number of parameter combinations analyzed by MOAT is significantly smaller than the 4^{17} combinations needed to sample the entire discretized parameter space. For each of the 24 initialization dates, we run a 3-day hindcast using each of the 180 combinations of input parameter values, resulting in 4,320 total simulations. This procedure is described in further detail in prior studies (e.g., Covey et al., 2013; Morales et al., 2019; Nardi et al., 2022; C. M. Zarzycki & Ullrich, 2017).

By perturbing an input parameter one-at-a-time, the MOAT method quantifies how the model output changes due to modifying that input alone. Here, "output" refers to a model simulation result, such as precipitation magnitude or global mean cloud fraction. By perturbing the value over multiple MOAT paths, we can derive a distribution of "elementary effects" d_{ijm}, the change in an output metric y_j due to perturbing input parameter x_i over path m (Equation 1 in Morales et al., 2019). Here, we quantify a parameter's influence on a given output metric using two measures: μ^*_{ij} and f_{ij+}. μ^*_{ij} is the average magnitude among the distribution of elementary effects for input parameter x_i and output metric y_j and characterizes the average response of the output metric to perturbing the input parameter value (Equation 4 in Covey et al., 2013). f_{ij+}, the monotonicity of the response, is the frequency with which increasing the input parameter x_i increases the output metric y_j (Equation 9 in Nardi et al., 2022). Together, these sensitivity measures provide information about the magnitude and direction of the output's response to a change in the input parameter value. Parameters with high μ^*_{ij} and f_{ij+} values near 0 or 1 are important and consistent in driving changes to the output. However, parameters with low μ^*_{ij} and f_{ij+} near 0.5 are unimportant and

inconsistent. Additional details about these metrics can be found in Nardi et al. (2022). To calculate elementary effects and sensitivity metrics, we employ the Sensitivity Analysis Library (SALib) (J. Herman & Usher, 2017).

3. Results

3.1. Assessing Validity of Sensitivity Metrics

We first evaluate the average magnitude $\left(\mu_{ij}^{*}\right)$ and direction $\left(f_{ij+}\right)$ of the response for various CAM6 output metrics at $t = 72$ hr. For each of the 180 unique parameter combinations, we first time-average model output fields over the 24 unique initializations. We then spatially average each of the 180 time-averaged fields, using cosine-latitude weighting, over two regions: (a) the Southern Storm Track, covering 0–360°E and 70-40°S, and (b) the Tropics, covering 0–360°E and 30°S-30°N. This results in a set of 180 time and spatially-averaged output metrics representing each unique combination of input parameter values. We then calculate the elementary effect d_{ijm} for each input x_i, output y_j, and path m. From these elementary effects, we can derive the μ_{ij}^{*} and f_{ij+} for each input x_i and output y_j.

Figure 1a ranks each input parameter (vertical axis) based on its μ_{ij}^{*} value for output metrics characterizing cloud feedbacks (horizontal axis). Table 1 provides descriptions of the input parameters, while Table 2 provides a key defining the output metrics analyzed in this study. We average output metrics over the Southern Storm Track (for the Tropics, see Figures S1–S3 in Supporting Information S1). The shading represents the input parameter's influence on the output metric relative to the other input parameters. For example, *micro_mg_accre_enhan_fact* (light yellow, #1) produces the highest-magnitude response in SWCF (leftmost column in Figure 1), while *C_invrs_tau_N2* produces the lowest-magnitude response in SWCF (dark purple #17). Figure 1b depicts the monotonicity f_{ij+}, the frequency with which increasing the input parameter increases the output metric over the Southern Storm Track. For instance, increasing *clubb_C11* increases low cloud percentage (second column from the left) approximately 90% of the time (dark red, 0.9), while increasing *micro_mg_accre_enhan_fact* never increases (i.e., always decreases) low cloud percentage (dark blue, 0.0). Meanwhile, increasing *C_invrs_tau_N2* only increases low cloud percentage 50% of the time (white, 0.5). Note that $1 - f_{ij+}$ represents (a) the probability that *decreasing* the input parameter increases the output metric and (b) the probability that increasing the input parameter *decreases* the output metric.

Parameters such as *micro_mg_accre_enhan_fact*, *clubb_C11*, *clubb_C8*, and *C_invrs_tau_N2_xp2* are broadly influential for cloud-radiative metrics, providing a relatively high-magnitude response in a consistent direction. Increasing *micro_mg_accre_enhan_fact*, a PUMASv1 parameter that acts as a multiplicative factor in the formulation of accretion, increases ice hydrometeor growth, which according to Figure 1b results in a consistent decrease in cloud percentage. *clubb_C11* and *clubb_C8* are both damping coefficients in the formulation of the third-order moment of vertical velocity $\overline{w'^3}$, a proxy for the skewness of the PDF for vertical velocity in CLUBBX that modulates the modeled low cloud regime (e.g., Guo et al., 2015). Increasing these input parameters increases damping and reduces $\overline{w'^3}$, which produces more of a stratocumulus regime (i.e., higher low cloud percentage compared to a cumulus regime) (Guo et al., 2014, 2015; Qian et al., 2018). We find a similar response of cloud percentage to increasing *clubb_C11* and *clubb_C8* in the second column of Figure 1b. *C_invrs_tau_N2_xp2* is a coefficient in the formulation of the dissipation term $\frac{1}{\tau_{x'2}}$ in the budget for scalar variances (e.g., $\overline{r_t'^2}$ and $\overline{\theta_l'^2}$). Increasing this coefficient increases dissipation in stably-stratified environments, thus reducing scalar variances. Figure 1 indicates that this results in a consistent increase in cloud percentage.

Though primarily interested in momentum flux and low-level wind profiles in CAM6-CLUBBX, we initially analyze cloud-radiative metrics that have been assessed in prior PPEs, thus providing a means of validating our analysis. Consistent with our findings, Guo et al. (2015) highlighted *clubb_C8* as an influential input parameter for low cloud percentage globally, with that parameter contributing 20–22% of the variation in global low cloud percentage in CAM5. Qian et al. (2018) found that *clubb_c8* was relatively influential for SWCF (related physically to low cloud percentage) in 3-day E3SM simulations. Specifically, they found that *clubb_c8* contributed 11–13% of the variation in global SWCF and 26–27% of the variation in SWCF over stratocumulus regions in the eastern Pacific Ocean.

Eidhammer et al. (2024) also found that in 3-year CAM6 simulations, *clubb_c8* was highly influential in fields such as SWCF and low cloud percentage. They also noted that microphysics parameters *micro_mg_accre_enhan_fact*,

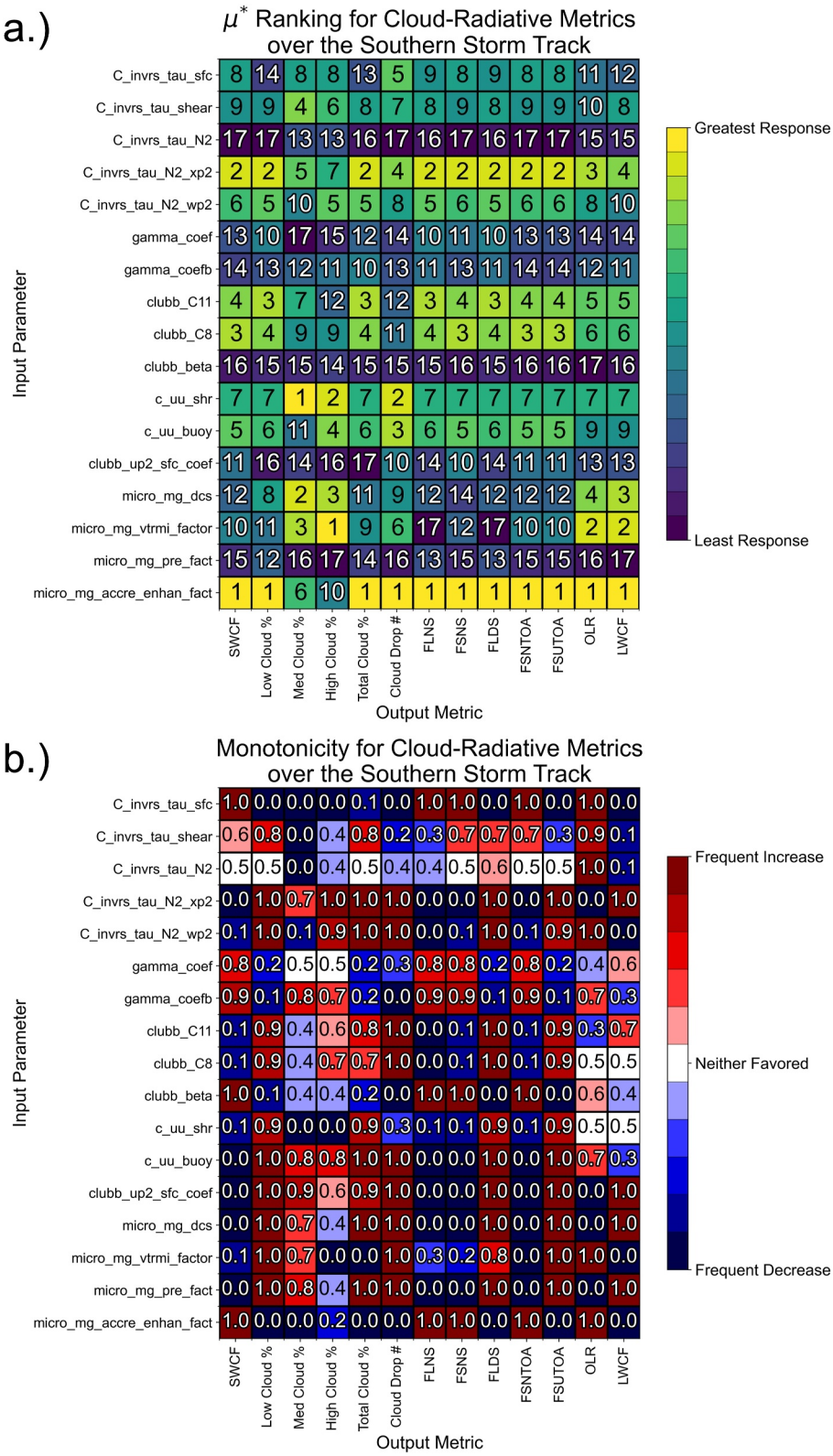

Figure 1.

micro_mg_dcs, and *micro_mg_vtrmi_factor* were influential for cloud feedbacks. This is consistent with our study, where *micro_mg_accre_enhan_fact* is broadly influential for many parameters, while *micro_mg_dcs* and *micro_mg_vtrmi_fact*, more tied to ice processes, are relatively influential for medium and high clouds. *C_invrs_tau_N2_xp2*, which is influential in our study, is an experimental parameter that has not been appreciably vetted in prior PPEs.

We also note some differences in our results compared to prior sensitivity analyses, namely in the relative influence of *clubb_C11* and *gamma_coef*. Though we find *clubb_C11* to be influential for cloud-radiative metrics, others (e.g., Eidhammer et al., 2024; Guo et al., 2015) found this parameter to be less important relative to other CLUBB parameters. Moreover, while Guo et al. (2015) and Qian et al. (2018) found *gamma_coef* to be relatively influential for low cloud percentage, we find that this parameter is not relatively influential in our analysis—consistent with Eidhammer et al. (2024).

We also compare the direction of the response for cloud-radiative metrics to those from prior studies. Overall, the directional responses of low cloud percentage and SWCF in Figure 1b compare favorably to the directional responses from prior PPEs. For example, our finding that low cloud percentage increases with an increase in *clubb_C8* and *clubb_C11*, and decreases with an increase in *gamma_coef*, is consistent with multiyear (e.g., Eidhammer et al., 2024; Guo et al., 2015) and short-term (e.g., Qian et al., 2018) PPEs. Given these results, we feel confident in the MOAT analysis' ability to highlight parameter sensitivities in metrics related to momentum flux in the PBL.

3.2. Identifying Influential Input Parameters

As in Nardi et al. (2022), we seek input parameters that have two key characteristics: (a) a relatively high-magnitude response in model output when perturbed (i.e., a high μ_{ij}^{*} ranking) and (b) a consistent directional response in model output (i.e., either a high or low f_{ij+}). A parameter with these characteristics offers confidence that perturbing this parameter in a given direction will produce the desired response in the output. We emphasize that the MOAT analysis is meant to provide a means of screening a large number of input parameters to identify a handful of influential parameters that merit additional analysis. Therefore, the forthcoming discussion is not designed to provide a definitive list of optimal input parameter values.

Figure 2 shows μ_{ij}^{*} and monotonicity for output metrics that characterize synoptic conditions and the general circulation, averaged over the Southern Storm Track. Several parameters produce a relatively high-magnitude response in a consistent direction for various synoptic output metrics. For example, *C_invrs_tau_shear* consistently produces relatively large responses in sea-level pressure (SLP), 2-m temperature (T_{2m}), and wind speed at the lowest model level (Figure 2a). (Herein, "wind speed" refers to the magnitude of the wind vector $\sqrt{\overline{u}^2 + \overline{v}^2}$). This parameter also produces consistent directional responses (Figure 2b). *C_invrs_tau_shear* is a coefficient in the experimental formulation of the eddy turnover time scale τ (C_{shear} in the third term on the r.h.s. of Equation 2) and modulates the degree of turbulent eddy dissipation due to vertical wind shear. In areas of high vertical wind shear (e.g., the Southern Storm Track), increasing this term is expected to increase eddy dissipation, with wind shear more effectively breaking up larger turbulent eddies into smaller ones (Mauritsen & Enger, 2008). Increasing *C_invrs_tau_shear* consistently decreases wind speed at the lowest model level (u_{bot}) but consistently increases wind speeds at higher levels (e.g., u_{500} through u_{4000}, the wind speeds at 500 m through 4,000 m). *c_uu_shr* produces a similar response, both in terms of average magnitude and direction of the response. *c_uu_shr* is a coefficient in the prognostic formulation of momentum flux that represents a pressure force that counters the turbulent production of momentum flux by vertical wind shear (third term on the r.h.s. of Equation 1). Similar to *C_invrs_tau_shear*, this parameter is expected to be influential where vertical wind shear is high, as in the Southern Storm Track.

Figure 1. In panel (a), μ^{*} for cloud-radiative output metrics. We average metrics over the Southern Storm Track region (0–360°E, 70-40°S) using cosine-latitude weighting. Light colors imply that the input parameter (vertical axis) produces a high-magnitude change in the output metric (horizontal axis) relative to other input parameters. For each output metric, we rank input parameters based on the magnitude of the response in the output metric. In panel (b), the frequency with which increasing the input parameter increases the output metric (i.e., the monotonicity). Deep reds (blues) imply that increasing the input parameter frequently increases (decreases) the output metric. For each combination of input parameter and output metric, the frequency is also plotted.

Table 2
Output Metrics Derived From CAM6 History Fields

Output metric	Description	Units
u_{bot}	Bottom model-level wind speed	$\frac{m}{s}$
T_{2m}	2-m air temperature	degrees K
q_{2m}	2-m specific humidity	$\frac{kg}{kg}$
Precip	Total precipitation rate	$\frac{m}{s}$
CAPE	Convective available potential energy	$\frac{J}{kg}$
ω_{700}	Vertical velocity (pressure coordinates) at 700 hPa	$\frac{Pa}{s}$
TPW	Total precipitable water	$\frac{kg}{m^2}$
SLP	Sea-level pressure	Pa
UXXX	Wind speed at XXX hPa	$\frac{m}{s}$
ZXXX	Geopotential height at XXX hPa	gpm
u_{xxx}	Wind speed at XXX meters	$\frac{m}{s}$
SWCF[a]	Shortwave cloud forcing	$\frac{W}{m^2}$
Low Cloud %	Vertically-integrated low cloud percentage	%
Med Cloud %	Vertically-integrated mid-level cloud percentage	%
High Cloud %	Vertically-integrated high cloud percentage	%
Total Cloud %	Vertically-integrated total cloud percentage	%
Cloud Drop	Vertically-integrated droplet number concentration	$\frac{1}{m^2}$
FLNS[a]	Net longwave flux at surface	$\frac{W}{m^2}$
FSNS[a]	Net solar flux at surface	$\frac{W}{m^2}$
FLDS[a]	Downwelling longwave flux at surface	$\frac{W}{m^2}$
FSNTOA[a]	Net solar flux at top of atmosphere	$\frac{W}{m^2}$
FSUTOA[a]	Upwelling solar flux at top of atmosphere	$\frac{W}{m^2}$
OLR[a]	Outgoing longwave radiation at top of model	$\frac{W}{m^2}$
LWCF[a]	Longwave cloud forcing	$\frac{W}{m^2}$
SHFLX	Sensible heat flux at surface	$\frac{W}{m^2}$
LHFLX	Latent heat flux at surface	$\frac{W}{m^2}$
$\overline{u'w'}$	Low-level vertical momentum flux	$\frac{m^2}{s^2}$
$\overline{\theta_l' w'}$	Low-level vertical flux of liquid water potential temperature (Larson, 2017)	$\frac{Km}{s}$
$\overline{r_t' w'}$	Low-level vertical moisture flux	$\frac{kg}{kg}\frac{m}{s}$
τ_{sfc}	Total surface wind stress	$\frac{N}{m^2}$
TKE	Low-level turbulent kinetic energy	$\frac{m^2}{s^2}$
τ_{zm}	Low-level eddy turnover time scale τ	$\frac{1}{s}$
K_h	Low-level effective vertical eddy diffusivity	$\frac{m^2}{s}$
L	Low-level vertical turbulent length scale	m
$\overline{w'^2}$	Low-level vertical velocity variance	$\frac{m^2}{s^2}$
PBLH	Boundary layer depth	m

Note. We average metrics over the region of interest using a cosine-latitude weighting. [a]Indicates output metrics that are daily averages (averaged over t = 48–72 hr). Otherwise, output metrics are instantaneous at t = 72 hr). "Low-level" refers to the second model level from the bottom.

Figure 3 similarly shows μ_{ij}^* and monotonicity for output metrics, averaged over the Southern Storm Track, that characterize turbulence in the PBL. As with the synoptic metrics, *C_invrs_tau_shear* and *c_uu_shr* broadly produce relatively large average responses in a consistent direction. Both are particularly influential for metrics that characterize vertical turbulent mixing, such as eddy turnover time scale τ and vertical momentum flux.

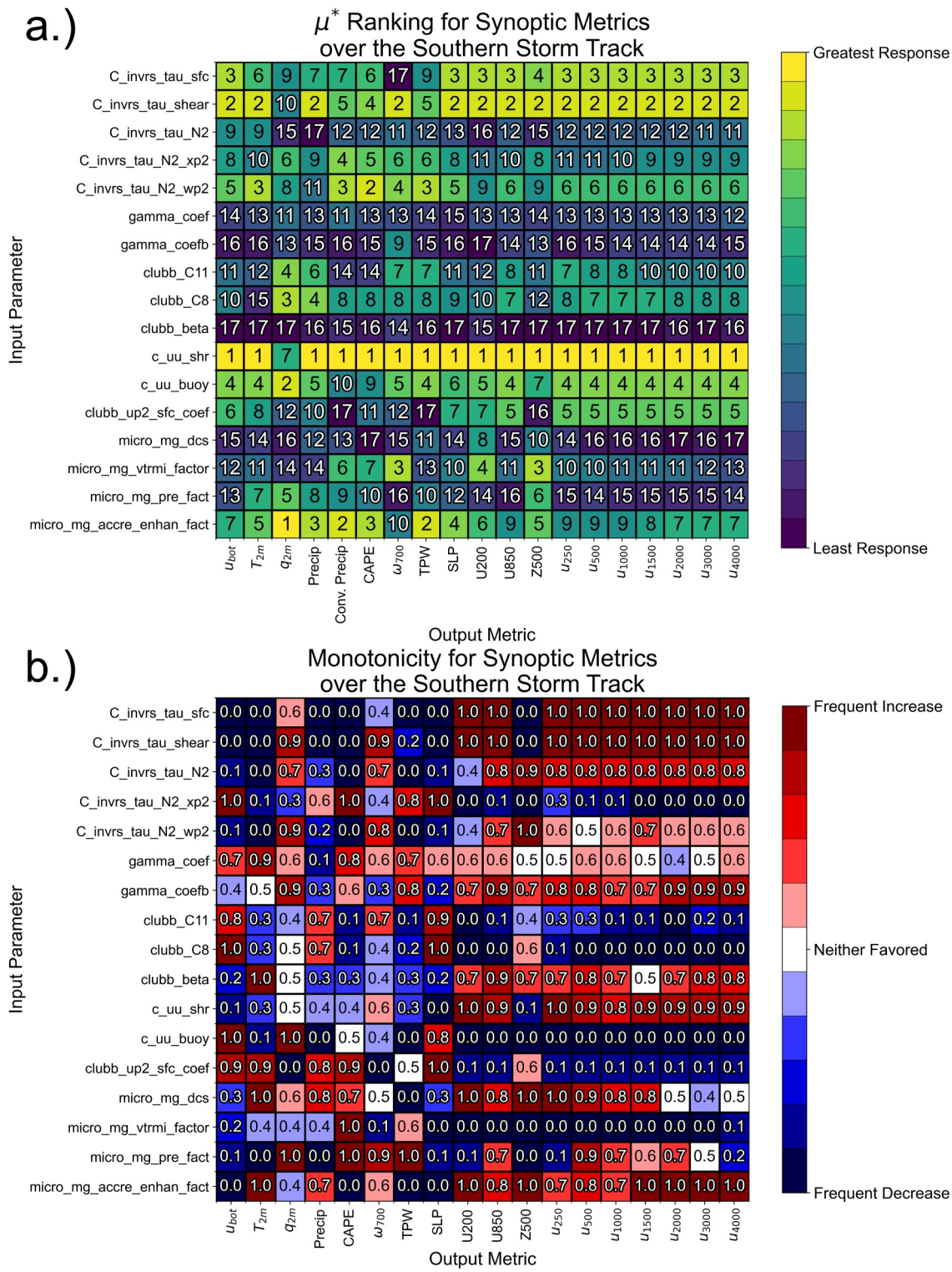

Figure 2. As in Figure 1, but for synoptic output metrics.

Increasing *C_invrs_tau_shear* results in a decrease of τ on the r.h.s. of Equation 1, thus increasing the speed with which the horizontal wind perturbation is relaxed toward zero, leading to enhanced damping of the momentum flux tendency. Physically, this represents reduced vertical turbulent mixing and momentum flux due to a breakup of larger turbulent eddies into smaller turbulent eddies. Increasing *c_uu_shr* similarly enhances damping of

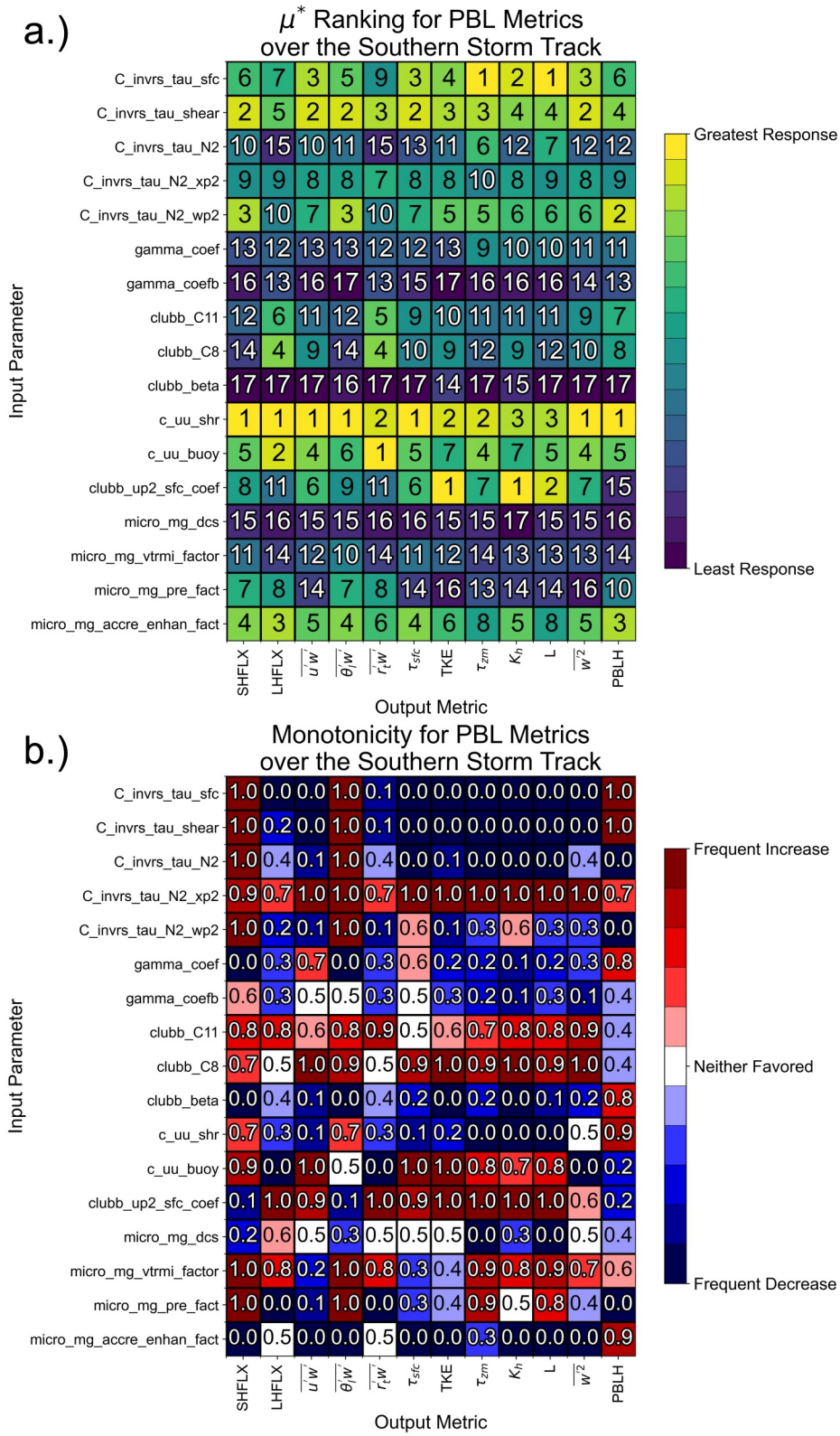

Figure 3. As in Figure 2, but for PBL output metrics.

turbulent production on the r.h.s. of Equation 1, thus decreasing turbulent fluxes (Figure 3b). The relatively high influence of *C_invrs_tau_shear* and *c_uu_shr* over the Southern Storm Track is consistent with Nardi et al. (2022), who demonstrated the importance of these parameters in the sheared environment of a TC.

Figures 1–3 only highlight the influence of CLUBBX parameters on regionally-averaged output metrics. We also seek to better understand the spatial variability of a parameter's influence, which is a key consideration for developers who want to reduce biases for a particular region, or phenomenon, without affecting the rest of the global climate. Here, we analyze how *C_invrs_tau_shear* affects low-level wind speed and surface wind stress (τ_{sfc} in plots, not to be confused with eddy turnover time scale τ) globally. Herein, surface wind stress refers to the magnitude of the surface wind stress vector, or the magnitude of the momentum flux vector at the surface: $\tau_{sfc} = \sqrt{\overline{u'w'}^2_{sfc} + \overline{v'w'}^2_{sfc}}$. We focus on *C_invrs_tau_shear* because it (a) produces a high-magnitude, directionally-consistent response in PBL wind and turbulence profiles and (b) has been shown in prior studies to be important for PBL structure in CAM6-CLUBBX (Nardi et al., 2022). Over the Southern Storm Track, where vertical wind shear is climatologically high, we hypothesize that increasing *C_invrs_tau_shear* will affect the low-level wind profile by modulating vertical turbulent mixing via eddy dissipation.

For a given initialization date, we perturb *C_invrs_tau_shear* once for each of the $M = 10$ MOAT paths. Over 24 initialization dates, this results in 240 total combinations where we perturb *only C_invrs_tau_shear* and all other parameters remain constant. After locating the 240 pairs of configurations along the MOAT paths where only *C_invrs_tau_shear* is perturbed, we put the configurations with the lower value of *C_invrs_tau_shear* into one group and the configurations with the higher value into a second group. The first group is effectively a distribution of simulations *before increasing C_invrs_tau_shear*, while the second is a distribution of simulations *after increasing C_invrs_tau_shear*. We emphasize that both groups have the same distribution of 24 initial conditions and $M = 10$ background input parameter values.

The left panels of Figure 4 show the change in wind speed at the lowest model level (u_{bot}, a) and surface wind stress (c) when increasing *C_invrs_tau_shear*. This is the difference between the 2D output field, averaged over the 240 perturbations, *before* increasing *C_invrs_tau_shear* and *after* increasing *C_invrs_tau_shear*. The right panels of Figure 4 show, at each latitude, the zonally-averaged difference in average u_{bot} (b) and surface wind stress (d) when increasing *C_invrs_tau_shear*. Figure 4 indicates that u_{bot} decreases globally when increasing *C_invrs_tau_shear*, especially over the Southern Storm Track. Meanwhile, panel c shows a decrease in surface wind stress at most locations globally, especially over the Southern Storm Track. The qualitatively-similar responses in u_{bot} and surface wind stress are consistent with bulk aerodynamic theory, where surface wind stress is directly proportional to wind speed above the surface (Stull, 1988). The magnitude of the response in u_{bot} and surface wind stress appears to be maximized over the higher latitudes and minimized over the tropics, especially in marine environments such as the Pacific Ocean. As expected, the areas of higher-magnitude response are spatially correlated (not shown) with vertical wind shear.

Figure 2 indicates that increasing *C_invrs_tau_shear* consistently increases wind speeds aloft (e.g., u_{xxx} from 250 to 4,000 m, U850, U200) with a high μ^*_{ij} and a positive $\not{f}_{ij+}$, while also decreasing SLP and 500-hPa geopotential height (Z500) over the Southern Storm Track. This implies that *C_invrs_tau_shear* potentially influences not just the PBL, but also the general circulation, even at 3 days. Specifically, the increased winds above the surface and decreased SLP in Figure 2 hint at an enhanced pressure gradient and stronger storm systems over the Southern Storm Track, yet despite this, Figure 4 shows that wind speed at the lowest model level *decreases*. We hypothesize that this opposing response between the lowest model level and model levels above is the result of a change in vertical momentum flux due to increasing *C_invrs_tau_shear*.

3.3. Physical Basis for Parameter Sensitivity

We next explore the physical mechanisms that drive the impact of *C_invrs_tau_shear* on low-level wind profiles and surface wind stress. We hypothesize that this parameter affects low-level winds by modulating vertical turbulent mixing. *C_invrs_tau_shear* appears as C_{shear} in the formulation of $\frac{1}{\tau}$, the inverse of the eddy turnover time scale τ, which is a measure of turbulent eddy dissipation (Equation 2). Increasing *C_invrs_tau_shear* enhances eddy dissipation, and reduces the eddy turnover time scale τ, in the presence of vertical wind shear. This results in an increase in the magnitude of term #6 on the r.h.s. of Equation 1. This term represents the tendency of pressure perturbations to reduce the horizontal wind perturbation u' toward zero over a time scale τ (Larson

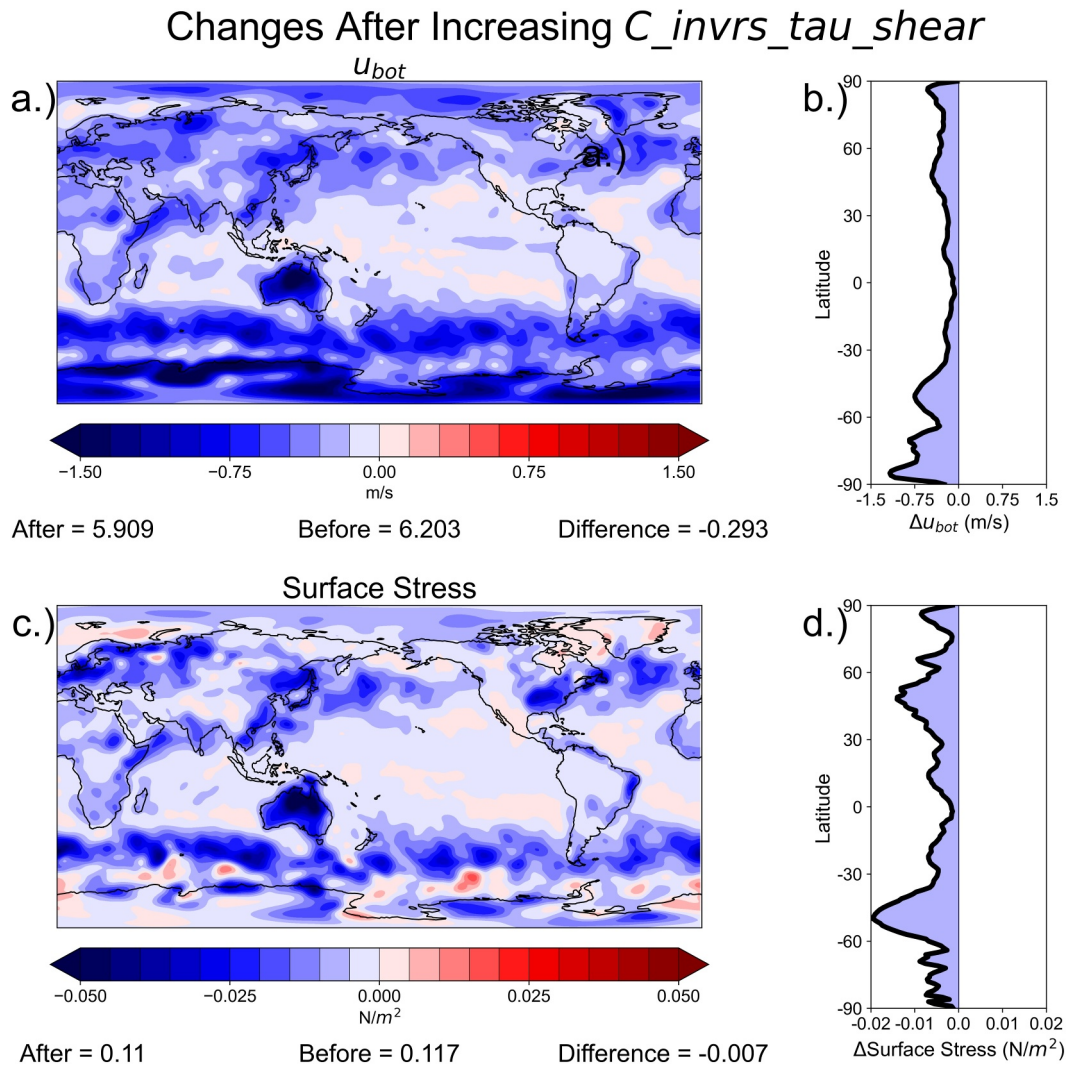

Figure 4. The change in u_{bot} (a) and surface wind stress (c) after increasing *C_invrs_tau_shear*. Reds (blues) indicate that increasing *C_invrs_tau_shear* increases (decreases) the output metric. For each output metric, the cosine-latitude-weighted global averages before and after increasing *C_invrs_tau_shear* are at the bottom of the panel. The panels on the right show the zonally-averaged change in u_{bot} (b) and surface wind stress (d) when increasing *C_invrs_tau_shear*.

et al., 2019). To remain consistent with Larson et al. (2019), we refer to this term as the "return-to-isotropy" term. A higher value of $\frac{1}{\tau}$ means that the force acts over a shorter time scale and more effectively damps the momentum flux tendency.

Figure 5 depicts the range, at each vertical level, of eddy dissipation due to wind shear (a), modeled eddy turnover time scale τ (b), and the return-to-isotropy term for the zonal component of momentum flux $\overline{u'w'}$ (c) before and after increasing *C_invrs_tau_shear*. The solid line represents the median of the distribution of 240 realizations at each vertical level, while the shading bounds the 25th and 75th percentiles of the distribution. Figure 5 provides a sense of how the distributions are shifting at each level in the 3-day hindcasts, over the Southern Storm Track, when increasing *C_invrs_tau_shear*. Shear-induced dissipation increases in Figure 5a, resulting in an increase in total turbulent eddy dissipation. This causes a shift in eddy turnover time scale τ, favoring smaller values, as seen in Figure 5b. With a decrease in τ, the pressure-induced relaxation of the horizontal wind perturbation toward zero occurs over a shorter time scale, causing a higher-magnitude damping of the time tendency of momentum flux (Figure 5c).

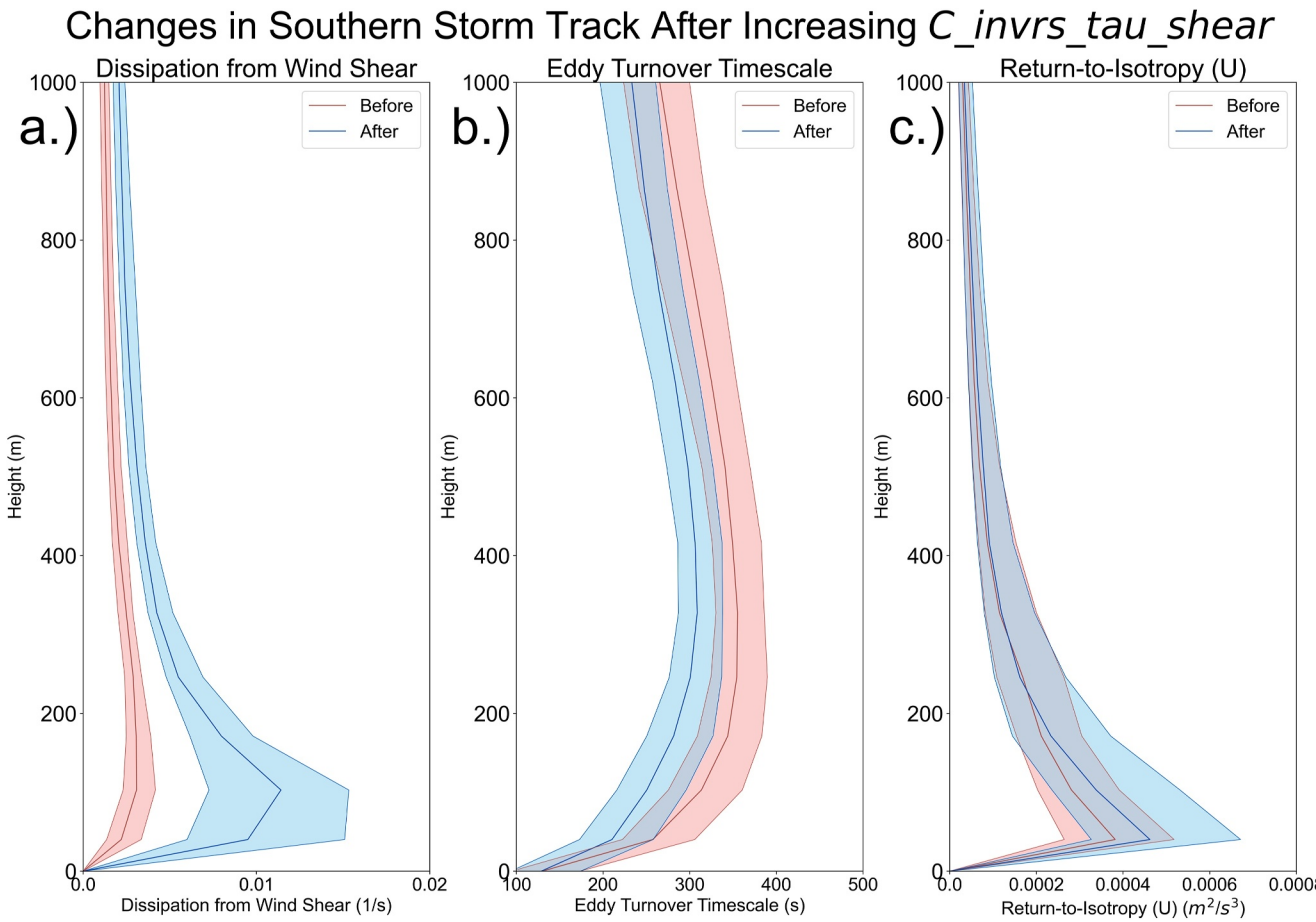

Figure 5. Distribution of eddy dissipation due to wind shear $\frac{1}{\tau_{shear}}$ (a), eddy turnover time scale τ (b), and the return-to-isotropy term for the zonal component of vertical momentum flux (c), at each vertical level, for configurations before (red) and after (blue) increasing *C_invrs_tau_shear*. Thicker lines denote the median value at each vertical level. The shaded region bounds the 25th and 75th percentiles. We derive the "before" distributions from the 240 simulations before increasing *C_invrs_tau_shear*, and we derive the "after" distributions from the 240 simulations after increasing *C_invrs_tau_shear*, with all else constant. For each simulation, we spatially average the metrics over the Southern Storm Track region (0–360°E, 70-40°S) with cosine-latitude weighting.

Figure 6 similarly shows the ranges for momentum flux (a), TKE (b), and wind speed (c) for the distributions before and after increasing *C_invrs_tau_shear*. (Herein, any plotted metric for momentum flux refers to the magnitude of the momentum flux vector $\sqrt{\overline{u'w'}^2 + \overline{v'w'}^2}$). With an increase in turbulent eddy dissipation and the return-to-isotropy pressure term, momentum flux magnitude decreases, mainly in the lowest model levels below 500 m, after increasing *C_invrs_tau_shear*. TKE is reduced due to decreased turbulent production of horizontal wind variances by vertical wind shear (Larson, 2017). Figure 6c indicates an increase in vertical wind shear at the lowest model levels when increasing *C_invrs_tau_shear*. Mathematically, as the return-to-isotropy damping term increases, the momentum flux budget in Equation 1 must achieve balance via the adjustment of other terms. In this case, the system attempts to balance itself by increasing wind shear $\left(\frac{\partial \overline{u}}{\partial z}\right)$ in the turbulent production term (term #3 on the r.h.s.). Physically, with less vertical turbulent mixing in the PBL, there is less downward transport of stronger winds aloft toward the surface.

The responses of PBL metrics to increasing *C_invrs_tau_shear* are consistent with the sensitivity metrics in Figure 3. The change in the wind speed profile over the Southern Storm Track due to an increase in *C_invrs_tau_shear* (Figure 6c) is also consistent with the responses predicted by MOAT (Figure 2b). The wind response, especially above 200 m, is specifically consistent with an enhanced pressure gradient and geostrophic wind aloft over the Southern Storm Track (Figure 2). We speculate that the decrease in wind speed at the lowest model level is driven by increased vertical wind shear caused by reduced vertical turbulent mixing, thus opposing

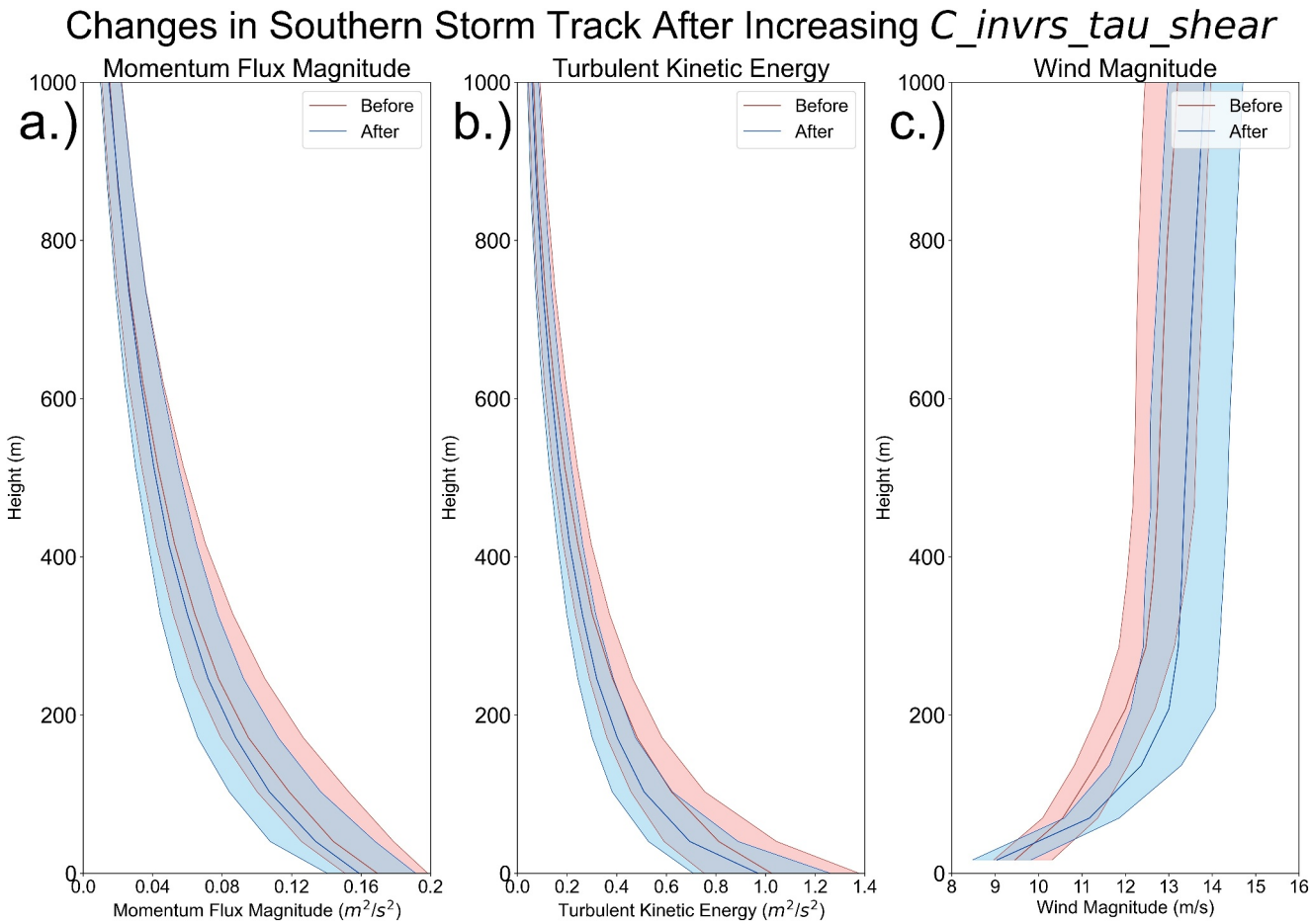

Figure 6. Same as Figure 5, but for momentum flux magnitude (a), TKE (b), and wind speed (c).

the effects of increased geostrophic winds above the PBL. Uncovering the exact nature of the nonlinear relationship between changes in momentum flux, wind speed, and pressure gradient within the PBL is a topic of future research. Nonetheless, we demonstrate here that the parameter sensitivities highlighted by the MOAT analysis indeed have a physical basis rooted in CLUBBX's closed, prognostic equations.

3.4. Targeted Parameter Perturbations in 20-Year Simulation

The MOAT method applied to 3-day simulations highlights several potential pathways toward modulating model output. Next, we investigate the degree to which the MOAT analysis can inform targeted parameter perturbations in multidecadal simulations. Prior studies (Ma et al., 2014; Qian et al., 2018; Wan et al., 2014; Xie et al., 2012) have indicated that parameters influence output metrics in similar ways for both 3-day and multi-year simulations. Here, we illustrate how model developers could hypothetically apply our 3-day MOAT analysis to achieve tangible impacts on various aspects of model behavior.

We run two 20-year simulations of CAM6-CLUBBX, one baseline simulation and one with two experimental parameter perturbations. In making perturbations, we seek to (a) reduce surface wind stress over the Southern Storm Track and (b) increase SWCF over the Tropics, a location where ESM cloud biases are common (e.g., Kay et al., 2012; Trenberth & Fasullo, 2010; Vignesh et al., 2020). Although motivated by biases, this is an illustrative example and does not necessarily reflect a suggested operational outcome for the model. In choosing these two outcomes, we wish to highlight two climate phenomena that are not directly related and occur in distinct regions. We simultaneously perturb multiple parameters in this example to illustrate a more realistic operational strategy of tuning multiple parameters at a time. In this exercise, we compare, between 3-day and 20-year simulations, how

Table 3
Baseline Values for the 20-Year CAM6-CLUBBX Simulations

Parameter	Baseline value
C_invrs_tau_sfc	0.05
C_invrs_tau_shear	**0.22 (0.33)**
C_invrs_tau_N2	0.3
C_invrs_tau_N2_xp2	0
C_invrs_tau_N2_wp2	0.1
gamma_coef	0.25
gamma_coefb	0.32
clubb_C11	0.5
clubb_C8	**0.8 (0.4)**
clubb_beta	2.0
c_uu_shr	0.1
c_uu_buoy	0
clubb_up2_sfc_coef	2.0
micro_mg_dcs	5×10^{-4}
micro_mg_vtrmi_factor	1.0
micro_mg_pre_fact	1.0
micro_mg_accre_enhan_fact	1.0

Note. We denote in bold the parameters perturbed in the targeted perturbations (perturbed values are in parentheses).

the parameter perturbations affect (a) the output metrics of interest (surface wind stress and SWCF) and (b) the physical mechanisms driving the output metrics.

Table 3 shows the parameter settings for these two configurations. The baseline configuration, which is comprised of the default parameter values used in our study, produces a realistic mean climate (e.g., a climate broadly similar to that in Danabasoglu et al., 2020). The parameter perturbations include changes to two CLUBBX parameters: an increase in *C_invrs_tau_shear* and a decrease in *clubb_C8*. Figures 3–6 indicate that increasing *C_invrs_tau_shear* produces a decrease in surface wind stress over the Southern Storm Track due to a reduction in vertical turbulent mixing and decreased near-surface wind speed. Meanwhile, Figure 1 indicates that *C_invrs_tau_shear* is less influential (relative to other input parameters) for SWCF but that *clubb_C8 is* relatively influential for SWCF, namely due to a high impact on low cloud percentage. Based on the MOAT method, decreasing *clubb_C8* is expected to decrease cloud cover and increase SWCF over the Southern Storm Track and Tropics (Figure S1 in Supporting Information S1). Physically, this represents weakened pressure damping of $\overline{w'^3}$, higher skewness in the distribution of vertical velocity, and a preference for cumulus versus stratocumulus clouds. Moreover, *clubb_C8* is less influential for surface wind stress (Figure 3). Each input parameter has an appreciable impact on one targeted output metric but less of an influence on the other. Therefore, we hypothesize that, in the 20-year simulations, increasing *C_invrs_tau_shear* will drive changes in PBL winds in the Southern Storm Track, while decreasing *clubb_C8* will drive changes in clouds and SWCF in the Tropics.

We run the 20-year simulations with fixed, prescribed SSTs and sea ice consistent with the present day (the "F2000climo" compset, see Open Research). Other than the targeted perturbations listed above (increased *C_invrs_tau_shear* and decreased *clubb_C*8), these two configurations are identical. We store output as monthly averages and average over years 2 through 20. We remove year 1 from the analysis to allow for model spinup. Figure 7 shows the difference between the perturbed and baseline simulations for SWCF (a), low cloud percentage (c), and low-level $\overline{w'^3}$ (e). Panels on the right side of Figure 7 (b, d, and f) show the zonally-averaged difference at each latitude. SWCF increases (i.e., clouds become "dimmer") almost everywhere, most notably in the Tropics, the equatorward flank of the Southern Storm Track, and the western coasts of continents. We focus primarily on responses over the ocean, where the increase in SWCF is well correlated spatially with a decrease in low cloud percentage, as well as an increase in low-level $\overline{w'^3}$. This is consistent with the 3-day MOAT results, which indicate that decreasing *clubb_C8* produces a decrease in cloud cover and an increase in SWCF. Physically, this is consistent with reduced pressure damping of the time tendency of $\overline{w'^3}$, resulting in enhanced skewness and a preference for cumulus clouds. (Factors driving responses over land are a subject of future research.) This is an example of consistent parameter sensitivity between the 3-day and 20-year simulations, thus indicating potential utility of the 3-day MOAT analysis for reducing cloud biases in longer-term simulations.

Figure 8 similarly shows the difference in u_{bot} (a-b), surface wind stress (c, d), and SLP (e, f) between the perturbed and baseline simulations. The MOAT analysis for the 3-day simulations indicates that increasing *C_invrs_tau_shear* results in a decrease in surface wind stress almost everywhere, especially over the Southern Storm Track (Figure 4). However, when making the targeted perturbations in the 20-year simulations, this reduction as a function of latitude is weaker. There are even prominent areas of increased surface stress over the Southern Storm Track, namely from Australia eastward toward South America. This increased surface stress is correlated spatially with an increase in wind speed at the lowest model level (u_{bot}) and an area of high-magnitude response in SLP. Figures 8e and 8f indicate an increase in pressure from Australia eastward toward South America, roughly near 40°S. Meanwhile, there is a strong decrease in pressure over the Southern Storm Track. This results in an enhanced pressure gradient as the climatological highs and lows in this region are strengthened.

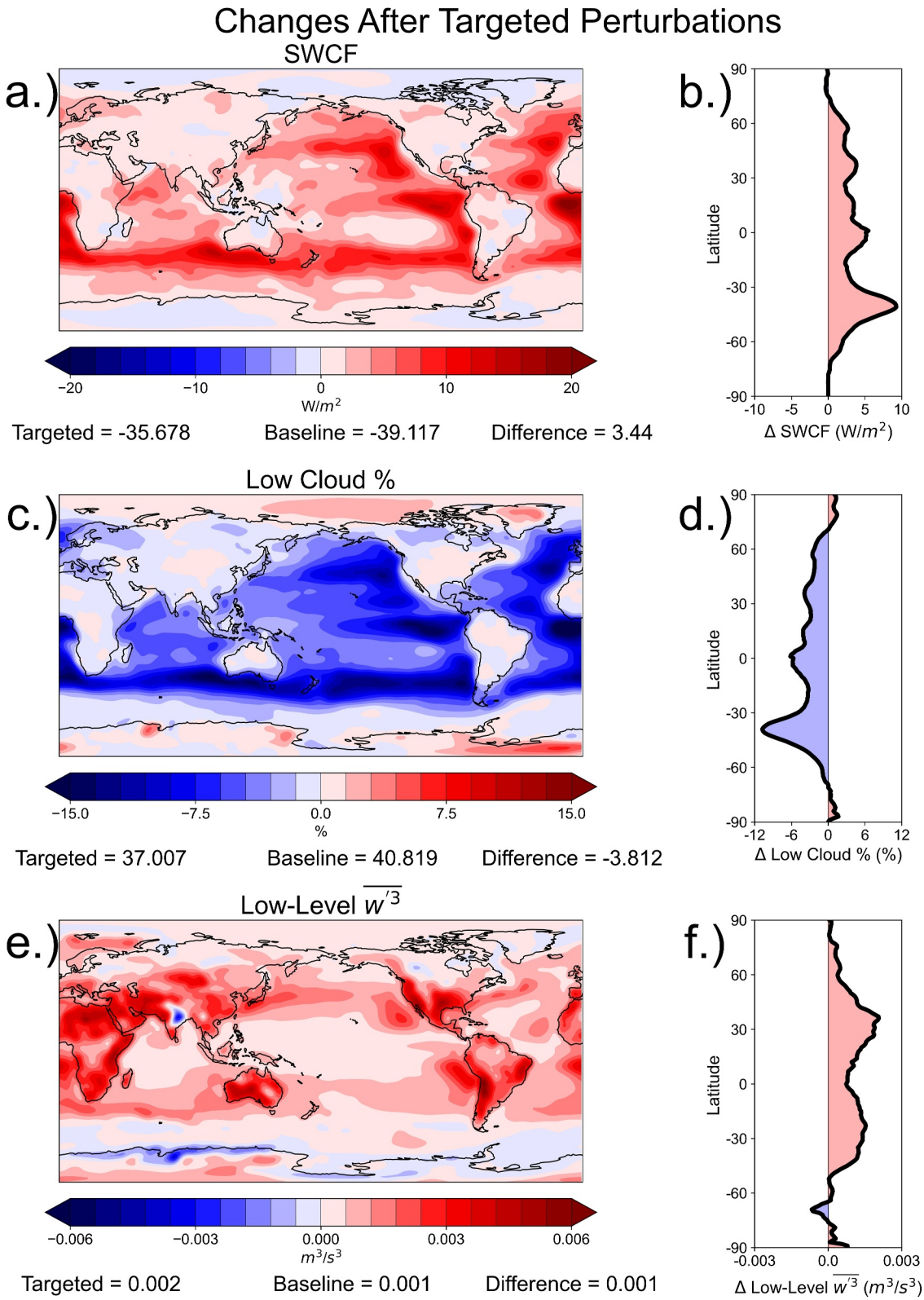

Figure 7.

The response in surface wind stress and low-level wind speed over the Southern Storm Track provides an example of a potential disconnect in regional parameter sensitivity between the 3-day and 20-year simulations.

Despite the difference in the response of the wind stress metric over the Southern Storm Track region, the 3-day and 20-year perturbations produce similar physical changes in the PBL. Owing to an increase in *C_invrs_tau_shear*, shear-induced eddy dissipation (Figure 9a) increases due to the increased coefficient C_{shear} on the r.h.s. of Equation 2. The increased shear-related eddy dissipation once again leads to a reduced eddy turnover time scale τ (Figure 9b), which in turn results in an increased pressure damping term (Figure 9c). Figure 10a highlights a slight decrease in momentum flux magnitude with the targeted parameter perturbations. The sign of the response is consistent with increased pressure damping of momentum flux, though the magnitude of the response is quite small. Consistent with decreased eddy turnover time scale τ, turbulent length scale, and momentum flux in the PBL, TKE is reduced (Figure 10b).

As in the 3-day simulations, to balance the momentum flux budget, the system responds to increased pressure damping by enhancing vertical wind shear (Figure 10c) in the turbulent production term. Physically, this represents reduced mixing downward of stronger winds toward the surface. However, the vertical wind shear responds to a lesser degree in the 20-year simulations. Figure 11 indicates that although wind speed at PBL top increases by a similar amount for both the 3-day and 20-year simulations, the magnitude of the wind shear increase is more muted in the 20-year simulations. As a result, the change in wind shear—albeit of the same directionality—does not lead to a clear reduction in near-surface wind speed and surface wind stress metrics. In this case, although the physical mechanisms modulated by the parameter perturbations are the same between the 3-day and 20-year simulations, coupled system feedbacks act to damp the magnitude of the response in the 20-year runs.

Analysis of the large-scale response to the targeted perturbations indicates nonlinear feedbacks due to changes in the general circulation. Figures 8e and 8f shows an appreciable response in SLP over the Southern Storm Track, while Figure 12 shows changes in fields of zonally-averaged zonal wind (a), meridional wind (b), temperature (c), and geopotential height (d). A modified general circulation can feed back into the PBL by influencing the adjustment of the various terms in the budgets of momentum and scalar fluxes, which are tied to characteristics of the environment. Though a response in the general circulation also appears in the 3-day simulations (e.g., Figure S10 in Supporting Information S1), a 20-year simulation allows more time for feedbacks to modulate fluxes within the PBL. Importantly, though responses in metrics associated with fast moist physics processes (e.g., clouds) are consistent between the 3-day and 20-year simulations, it is possible that with short-term simulations, there is not enough time for dynamical metrics to fully adjust to climate system feedbacks manifesting over longer timescales. Acquiring a deeper understanding of the physical mechanisms driving the response in the general circulation is a key objective of future research.

4. Discussion and Conclusions

In this study, we perform an interpretable sensitivity analysis using the MOAT method on 3-day, initialized hindcasts in CAM6 with an experimental configuration of CLUBB (CAM6-CLUBBX). We build on prior analyses of CLUBB parameter sensitivities in ESMs (e.g., Eidhammer et al., 2024; Guo et al., 2014, 2015; Qian et al., 2018), which have mainly focused on cloud-radiative metrics and have not included new tunable parameters related to experimental formulations of momentum flux and eddy dissipation. We further extend prior CLUBB sensitivity studies by examining physical mechanisms driving specific parameter sensitivities, especially as they relate to momentum flux in the PBL. Furthermore, given prior studies demonstrating that short-term simulations provide useful information about parameter sensitivity in multiyear simulations (Qian et al., 2018), we explore how the 3-day MOAT analysis can help guide targeted parameter perturbations in 20-year CAM6-CLUBBX simulations.

Figure 7. The change in SWCF (a), low cloud percentage (c), and the third-order moment of vertical velocity $\left(\overline{w'^3}\right)$ after making two targeted parameter perturbations in a 20-year simulation. Reds (blues) indicate that the simulation with the targeted perturbations produces a larger (smaller) value of the parameter compared to the baseline 20-year simulation. For each output metric, the cosine-latitude-weighted global averages before and after making the targeted perturbations are located at the bottom of the panel. We average the output over years 2 through 20 of each simulation. The panels on the right show the zonally-averaged change in SWCF (b), low cloud percentage (d), and $\overline{w'^3}$ (f) when making the targeted perturbations.

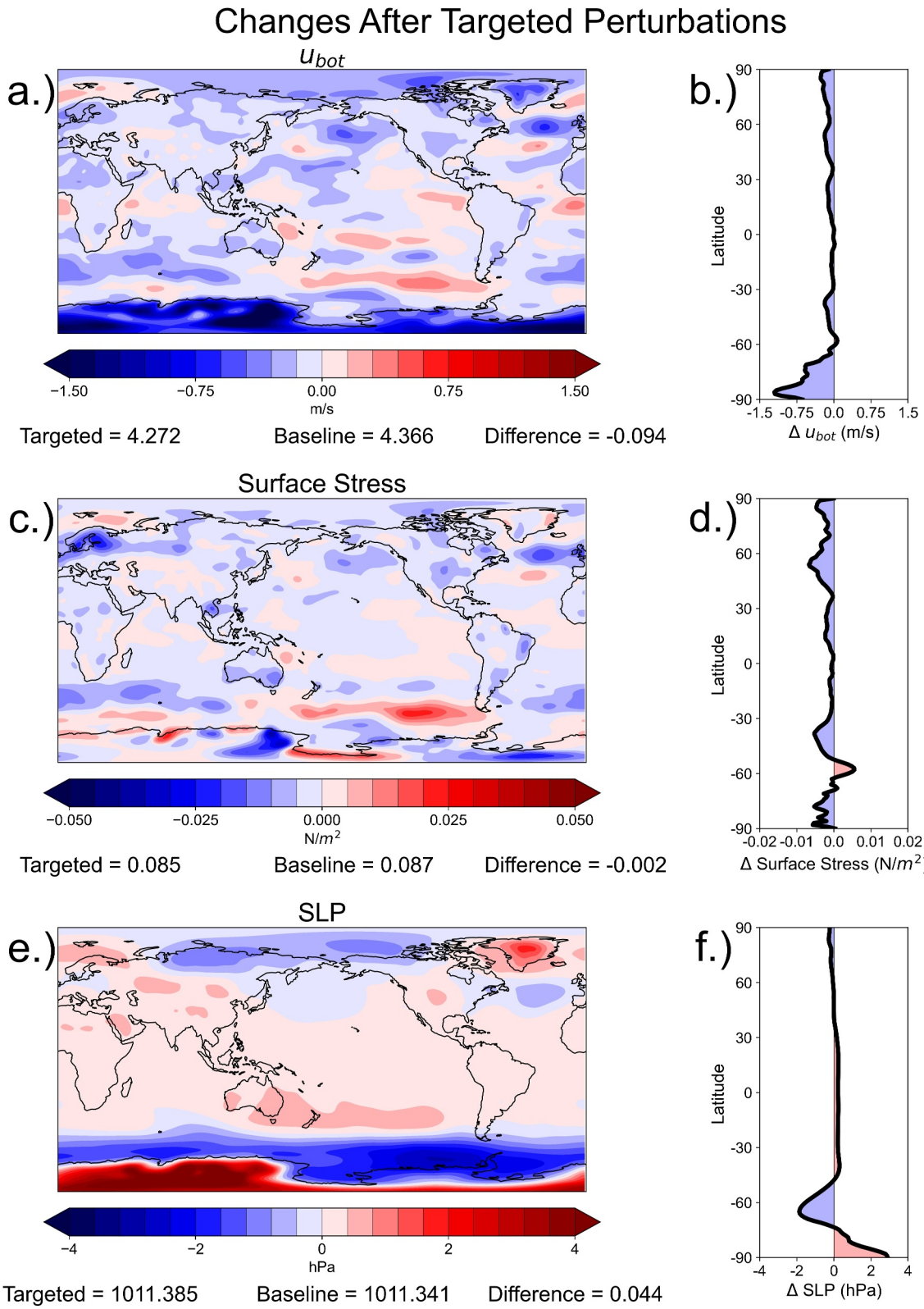

Figure 8. Same as Figure 7, but for u_{bot} (a–b), surface wind stress (c–d), and sea-level pressure (e–f).

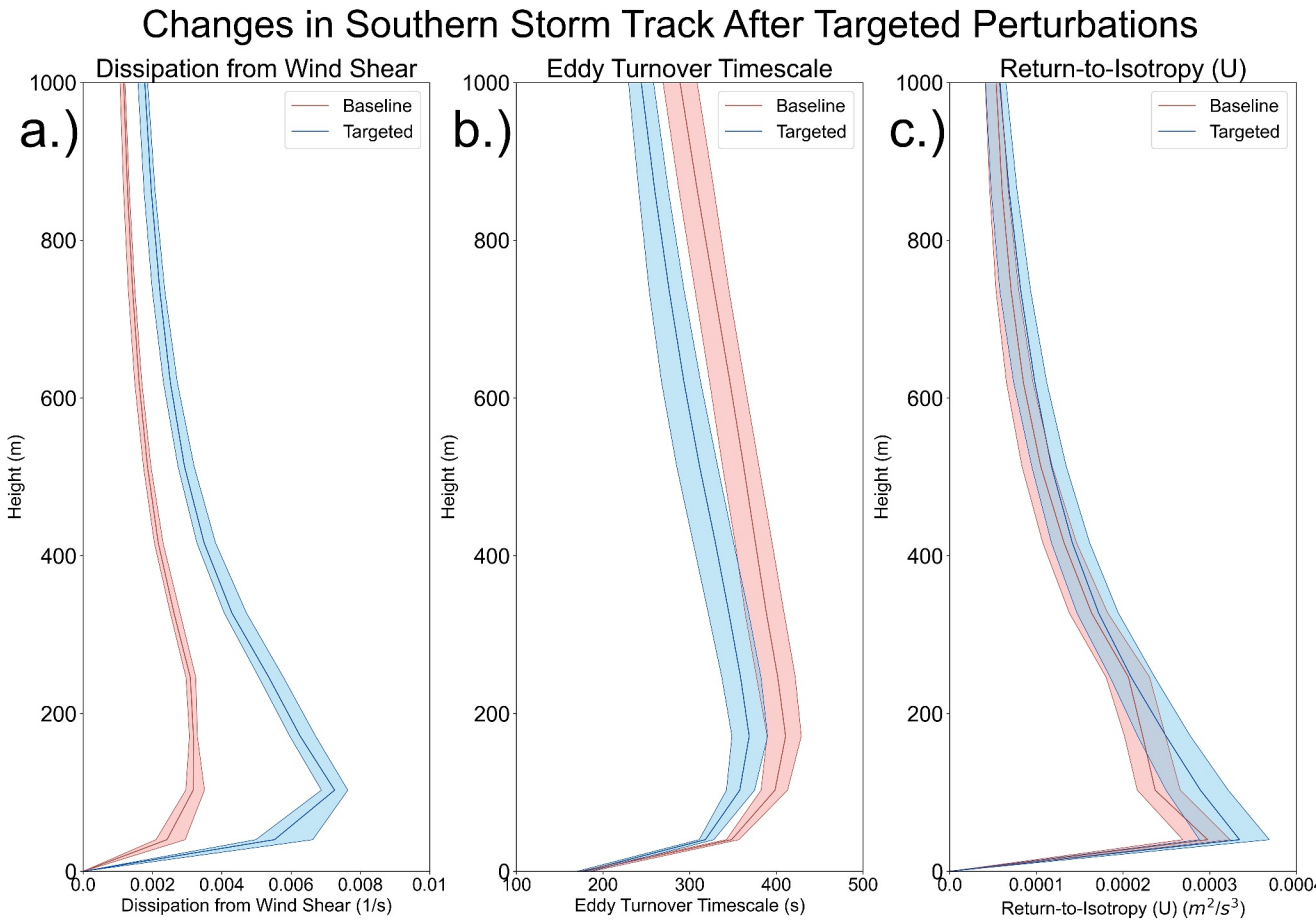

Figure 9. Distribution of eddy dissipation due to wind shear (a), eddy turnover time scale τ (b), and the return-to-isotropy term for the zonal component of vertical momentum flux (c), at each vertical level, for configurations before (red) and after (blue) making the targeted parameter perturbations. Thicker lines denote the median value at each vertical level. The shaded region bounds the 25th and 75th percentiles. For the perturbed and baseline configurations, we derive the distributions from monthly-averaged fields for each month during years 2 through 20 of each simulation. For each simulation, we spatially-average the metrics over the Southern Storm Track region (0–360°E, 70-40°S) with cosine-latitude weighting.

We find that parameter sensitivities in 3-day simulations compare favorably to prior studies that have explored the impact of CLUBB on cloud-radiative metrics in ESMs. Consistent with prior PPEs, *clubb_C8* and *clubb_C11*, both playing a role in estimating the third-order moment of vertical velocity $\left(\overline{w'^3}\right)$, are influential parameters for SWCF in the 3-day MOAT analysis (Figure 1). We then extend our analysis to output metrics related to the synoptic state and general circulation (Figure 2) and PBL turbulence (Figure 3). *C_invrs_tau_shear* and *c_uu_shr* stand out as parameters that affect PBL structure and the general circulation in short-term simulations. Both parameters appear in either the formulation of prognostic momentum flux or eddy dissipation and modulate the amount of vertical turbulent mixing in the PBL. Their importance in governing PBL structure is consistent with the findings of Nardi et al. (2022), who identified both parameters as key drivers of PBL structure in idealized TCs in CAM6-CLUBBX.

As they are new parameters, *C_invrs_tau_shear* and *C_uu_shr* have not been vetted in prior analyses, so our study provides an opportunity to get a better understanding of the impact these parameters have on various output metrics in an ESM. Therefore, we analyze how PBL structure changes when increasing one of these parameters (*C_invrs_tau_shear*). With an increase in *C_invrs_tau_shear*, eddy dissipation increases in the PBL, leading to reduced vertical turbulent mixing. As the system achieves balance in the momentum flux budget under reduced vertical turbulent mixing, PBL wind shear increases and results in a reduced near-surface wind speed (Figures 5 and 6). This results in reduced surface wind stress over the Southern Storm Track region, which is predicted by the MOAT analysis.

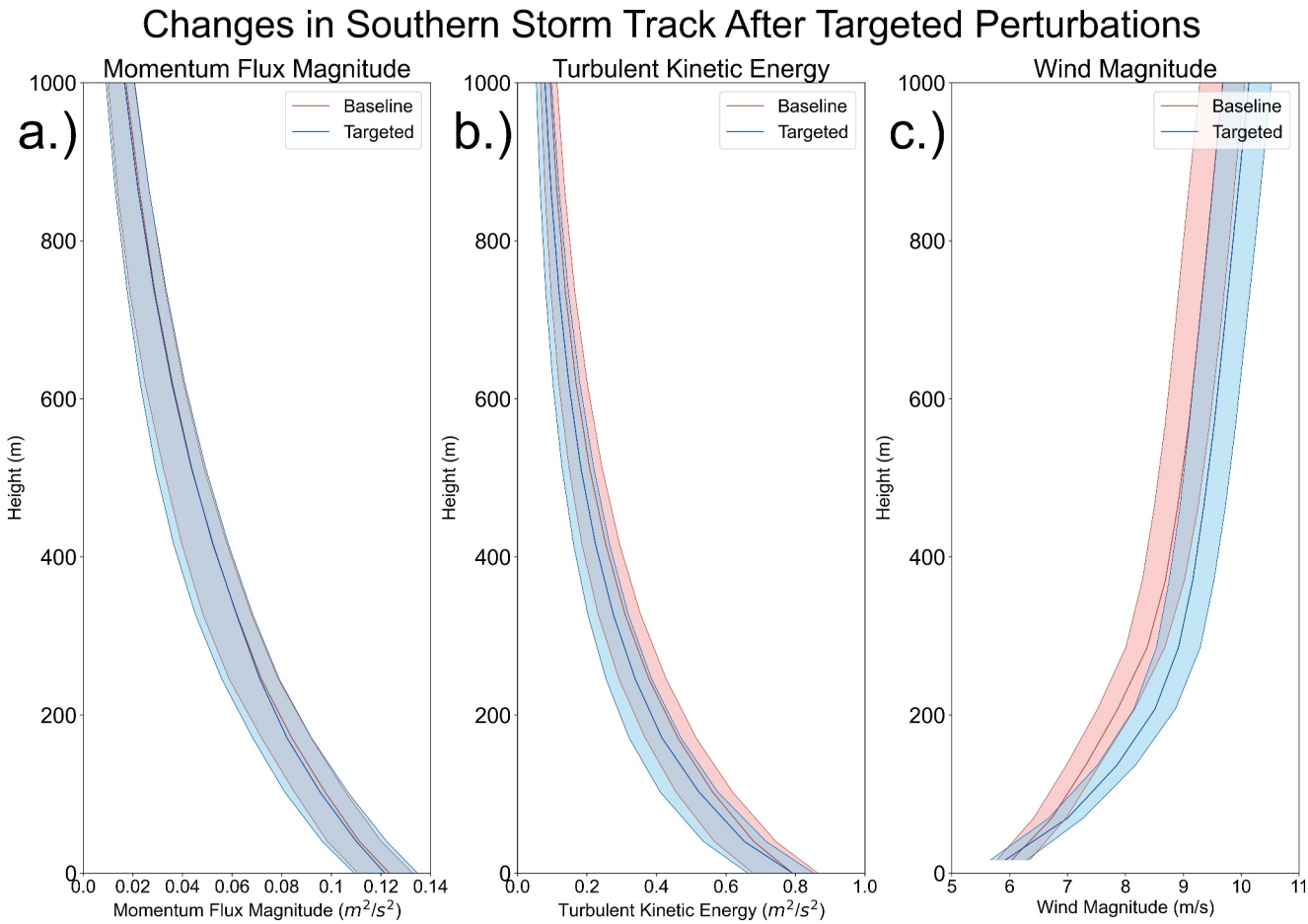

Figure 10. Same as Figure 9, but for momentum flux magnitude (a), TKE (b), and wind speed (c).

Finally, we evaluate whether the MOAT analysis using 3-day hindcasts can inform parameter perturbations to get desired responses in 20-year simulations. Based on sensitivity measures from MOAT, we make two targeted parameter perturbations: (a) increase *C_invrs_tau_shear* and (b) decrease *clubb_C8*, with the desired effect of decreasing surface wind stress over the Southern Storm Track and increasing SWCF over the Tropics. Making these two parameter perturbations produces a marked increase in SWCF over the Tropics (Figure 7), largely due to a decrease in cloud fraction caused by increasing *clubb_C8* and therefore reducing $\overline{w'^3}$. However, these targeted parameter perturbations result in essentially negligible changes over the Southern Storm Track (Figure 8), which is different from the response in the 3-day MOAT analysis. Though the increase in *C_invrs_tau_shear* produces a similar physical response in the PBL, namely a decrease in vertical mixing and increased vertical wind shear, climate feedbacks manifesting in the 20-year simulations reduce the magnitude of the wind shear response and therefore mute the response of the near-surface wind metrics.

The similar responses for SWCF are consistent with Qian et al. (2018), who demonstrated that certain CLUBB parameters such as *clubb_C8* affect cloud-radiative metrics in the same way for both 3-day and 5-year simulations. However, while this similarity may exist for moist physics processes (e.g., clouds), we find that this same correlation does not necessarily exist for PBL metrics that are governed by a balance of processes tied to winds, pressure gradients, etc. For example, we find that the targeted perturbations (Figure 12), and individual parameter perturbations (Figures S4–S9 in Supporting Information S1), affect the general circulation in the 20-year simulations. Though additional analysis is required in future studies, we speculate that the changes in the general circulation feed back into the PBL by affecting the balance of terms within the budgets of PBL fluxes (e.g., momentum flux). Though the individual parameters modulate the general circulation even at 3 days (e.g., Figures S10 and S11 in Supporting Information S1), 20-year simulations allow more time for changes in the mean state to

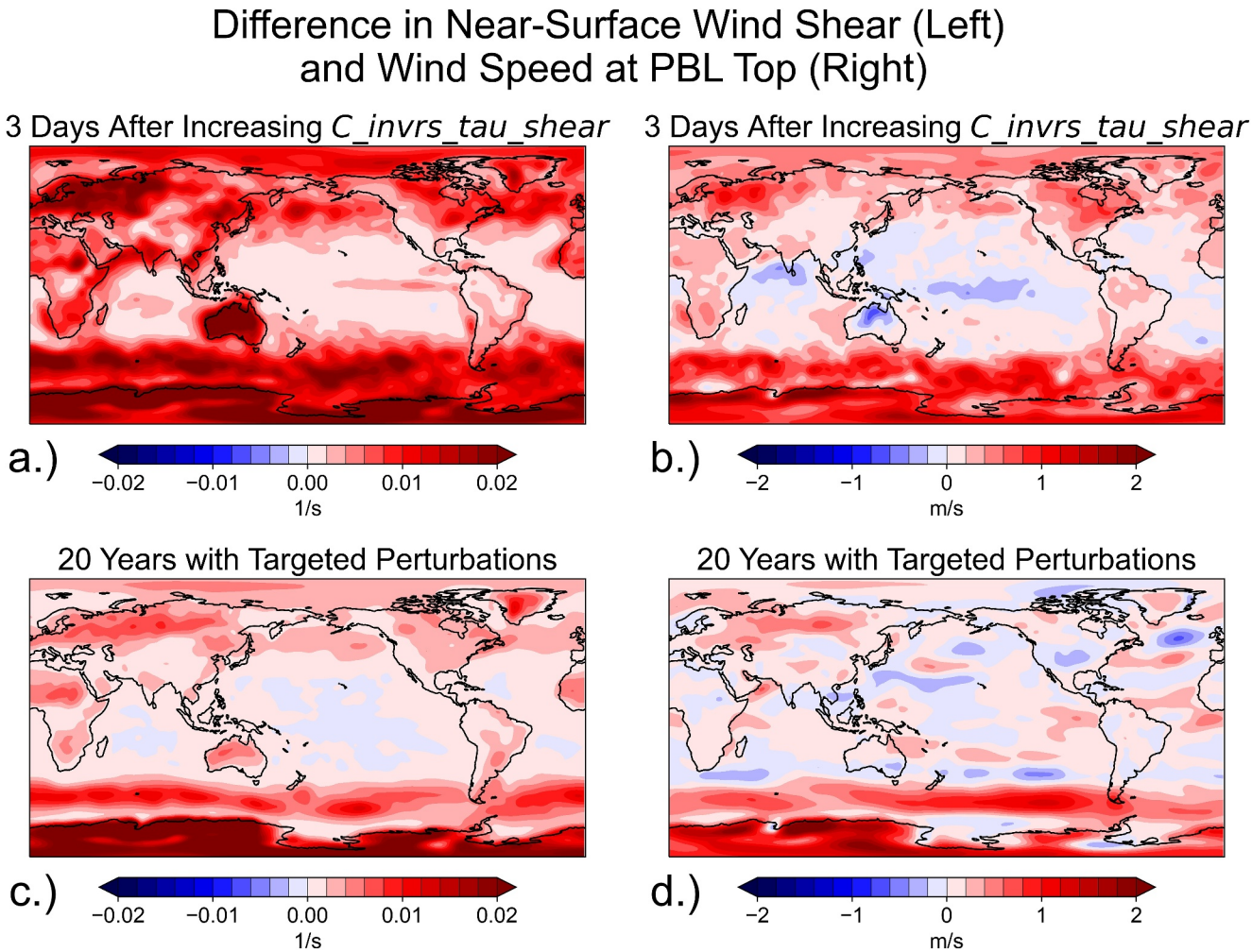

Figure 11. On the top row, the change in near-surface vertical wind shear (a) and wind speed at the top of the PBL (b) after 3 days when increasing *C_invrs_tau_shear*. On the bottom row, the change in near-surface vertical wind shear (c) and wind speed at the top of the PBL (d) after making the targeted perturbations in the 20-year simulations. Reds (blues) indicate that the field increases (decreases) when making these changes. The wind shear in panels (a, c) is the vertical gradient in the wind speed near the surface. The results for the 3-day simulations come from instantaneous model output for simulations before and after increasing only *C_invrs_tau_shear*. We derive the results for the 20-year simulations from monthly-average output over years 2 through 20.

affect how the terms in the momentum flux budget come into balance following the perturbation of an individual term (e.g., pressure damping). This discrepancy in allowed response time can then result in differences in the magnitude of the response in a metric such as vertical wind shear.

In the future, it will be important to get a deeper physical understanding of the mechanisms driving a parameter's influence in both the short-term and over multiple decades. For example, future studies should quantify and compare how each term in the momentum flux budget responds over different time scales. This can aid in better understanding how climate system feedbacks manifest for long-term simulations and affect CLUBBX parameter sensitivities. Future studies should also explore how our results vary when running coupled simulations with an interactive ocean. For example, changes in clouds can be amplified/dampened as the upper ocean responds to changes in the surface radiation budget.

We also emphasize that the MOAT analysis is meant to serve as an initial screening tool to separate a handful of influential input parameters from a larger set of tunable parameters. While MOAT possesses strengths highlighted here, it also contains drawbacks (Morales et al., 2019), including a limited quantification of the variance explained by each input parameter. Nonlinear feedbacks, which are inherent to a complex climate system, provide additional

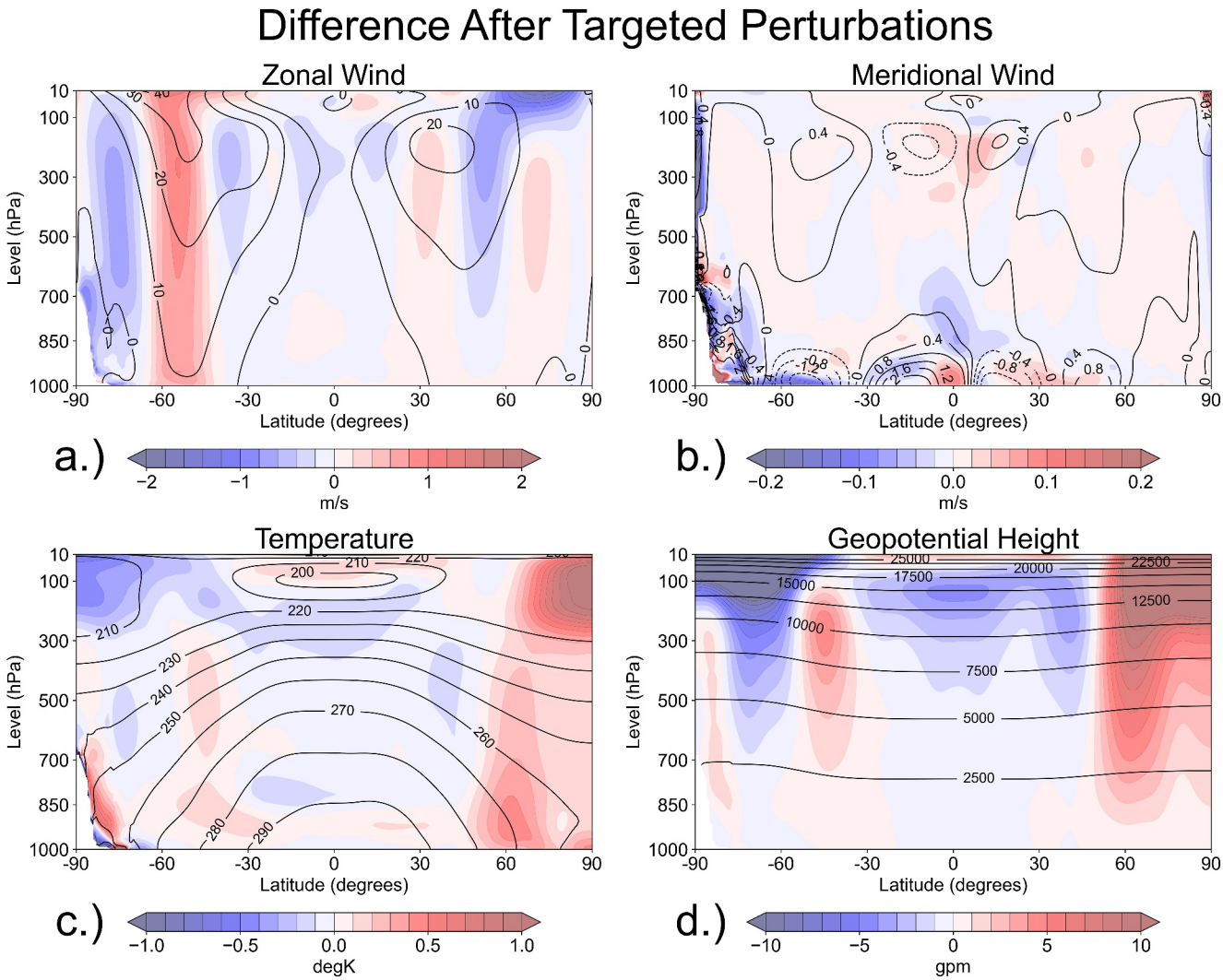

Figure 12. Cross-sections of the difference (shading) in zonally-averaged zonal wind (a), meridional wind (b), temperature (c), and geopotential height (d) when running the 20-year simulation with the targeted parameter perturbations. Reds (blues) indicate that the zonal average of the simulation with the targeted parameter perturbations has a larger (smaller) value of the output compared to the zonal average of the baseline. Black contours denote the zonally-averaged climatological values from the baseline configuration. White shading denotes null values where high terrain exists and no zonal averaging can be done.

challenges in interpreting the MOAT results (e.g., the multi-parameter perturbations in Section 3.4). Nonetheless, this study provides a framework through which model developers can identify important input parameters and perform additional analysis of the physical mechanisms tied to these parameters. This information can then provide guidance for developers to produce a model that is not only more accurate but also more realistic physically.

Data Availability Statement

Short and long-term sensitivity analysis is performed using a development release of the Community ESM version 2 (CESM2, Danabasoglu et al., 2020). The specific tag of CESM2 used in this study (6.3.124) is accessed via the portal referenced in ESCOMP (2023). More information about the compset used can be found in "CAM6.3 User's Guide" (2024). Parameter sensitivity analysis is conducted using the SALib in Python (SALib), which is an open-source software package (J. Herman & Usher, 2017). Betacast is open-source software available for public use and is documented in C. Zarzycki (2023). All model simulations, analysis data, and code supporting this manuscript are archived with Penn State Data Commons (Nardi et al., 2024).

Acknowledgments
This research is jointly funded as part of a Climate Process Team (CPT) under Grant AGS-1916689 from the National Science Foundation (NSF) and Grant NA19OAR4310363 from the National Oceanic and Atmospheric Administration (NOAA). We acknowledge computational support for this research from the Pennsylvania State University's Institute for Computational and Data Sciences' Roar Collab High Performance Computing Cluster (https://www.icds.psu.edu/roar-collab/). We also acknowledge computational support from NCAR's Cheyenne supercomputer (https://doi.org/10.5065/D6RX99HX), which is maintained by NCAR's Computational and Information Systems Laboratory (CISL) and sponsored by NSF. The authors thank Julio Bacmeister and Ben Stephens for providing feedback on this work.

References

Bacmeister, J. T., Reed, K. A., Hannay, C., Lawrence, P., Bates, S., Truesdale, J. E., et al. (2018). Projected changes in tropical cyclone activity under future warming scenarios using a high-resolution climate model. *Climatic Change*, *146*(3–4), 547–560. https://doi.org/10.1007/s10584-016-1750-x

Bacmeister, J. T., Wehner, M. F., Neale, R. B., Gettelman, A., Hannay, C., Lauritzen, P. H., et al. (2014). Exploratory high-resolution climate simulations using the Community Atmosphere Model (CAM). *Journal of Climate*, *27*(9), 3073–3099. https://doi.org/10.1175/JCLI-D-13-00387.1

CAM6.3 User's Guide. (2024). Retrieved from https://ncar.github.io/CAM/doc/build/html/users_guide/

Campolongo, F., Cariboni, J., & Saltelli, A. (2007). An effective screening design for sensitivity analysis of large models. *Environmental Modelling and Software*, *22*(10), 1509–1518. https://doi.org/10.1016/j.envsoft.2006.10.004

Chinta, S., Sai, J. Y., & Balaji, C. (2021). Assessment of WRF model parameter sensitivity for high-intensity precipitation events during the Indian Summer Monsoon. *Earth and Space Science*, *8*(6). https://doi.org/10.1029/2020EA001471

Covey, C., Lucas, D. D., Tannahill, J., Garaizar, X., & Klein, R. (2013). Efficient screening of climate model sensitivity to a large number of perturbed input parameters. *Journal of Advances in Modeling Earth Systems*, *5*(3), 598–610. https://doi.org/10.1002/jame.20040

Danabasoglu, G., Lamarque, J. F., Bacmeister, J., Bailey, D. A., DuVivier, A. K., Edwards, J., et al. (2020). The community Earth system model version 2 (CESM2). *Journal of Advances in Modeling Earth Systems*, *12*. https://doi.org/10.1029/2019MS001916

Dennis, J. M., Edwards, J., Evans, K. J., Guba, O., Lauritzen, P. H., Mirin, A. A., et al. (2012). CAM-SE: A scalable spectral element dynamical core for the community atmosphere model. *International Journal of High Performance Computing Applications*, *26*(1), 74–89. https://doi.org/10.1177/1094342011428142

Duffy, M. L., Medeiros, B., Gettelman, A., & Eidhammer, T. (2024). Perturbing parameters to understand cloud contributions to climate change. *Journal of Climate*, *37*(1), 213–227. https://doi.org/10.1175/JCLI-D-23

Eidhammer, T., Gettelman, A., Thayer-Calder, K., Watson-Parris, D., Elsaesser, G., Morrison, H., et al. (2024). An extensible perturbed parameter ensemble (PPE) for the Community Atmosphere Model Version 6. Retrieved from https://egusphere.copernicus.org/preprints/2024/egusphere-2023-2165/

ESCOMP. (2023). Community Earth system model release tag 6.3.124 [Software]. *Earth System Community Modeling Portal*. https://github.com/ESCOMP/CAM/releases/tag/cam6_3_124

Gettelman, A., Morrison, H., Eidhammer, T., Thayer-Calder, K., Sun, J., Forbes, R., et al. (2023). Importance of ice nucleation and precipitation on climate with the Parameterization of Unified Microphysics across Scales version 1 (PUMASv1). *Geoscientific Model Development*, *16*(6), 1735–1754. https://doi.org/10.5194/gmd-16-1735-2023

Golaz, J.-C., Larson, V. E., & Cotton, W. R. (2002). A PDF-based model for boundary layer clouds. Part I: Method and model description. *Journal of the Atmospheric Sciences*, *59*(24), 3540–3551. https://doi.org/10.1175/1520-0469(2002)059,3540:APBMFB.2.0.CO;2

Graap, S., & Zarzycki, C. M. (2024). Using EUREC4A/ATOMIC field campaign data to improve trade wind regimes in the Community Atmosphere Model. *Geoscientific Model Development*, *17*(4), 1627–1650. https://doi.org/10.5194/gmd-17-1627-2024

Guo, Z., Griffin, B. M., Domke, S., & Larson, V. E. (2021). A parameterization of turbulent dissipation and pressure damping time scales in stably stratified inversions, and its effects on low clouds in global simulations. *Journal of Advances in Modeling Earth Systems*, *13*(4). https://doi.org/10.1029/2020MS002278

Guo, Z., Wang, M., Qian, Y., Larson, V. E., Ghan, S., Ovchinnikov, M., et al. (2015). Parametric behaviors of CLUBB in simulations of low clouds in the Community Atmosphere Model (CAM). *Journal of Advances in Modeling Earth Systems*, *7*(3), 1005–1025. https://doi.org/10.1002/2014MS000405

Guo, Z., Wang, M., Qian, Y., Larson, V. E., Ghan, S., Ovchinnikov, M., et al. (2014). A sensitivity analysis of cloud properties to CLUBB parameters in the single-column Community Atmosphere Model (SCAM5). *Journal of Advances in Modeling Earth Systems*, *6*(3), 829–858. https://doi.org/10.1002/2014MS000315

Herman, J., & Usher, W. (2017). SALib: An open-source Python library for sensitivity analysis [Software]. *Journal of Open Source Software*, *2*(9), 97. https://doi.org/10.21105/joss.00097

Herman, J. D., Kollat, J. B., Reed, P. M., & Wagener, T. (2013). Technical note: Method of Morris effectively reduces the computational demands of global sensitivity analysis for distributed watershed models. *Hydrology and Earth System Sciences*, *17*(7), 2893–2903. https://doi.org/10.5194/hess-17-2893-2013

Hersbach, H., et al. (2017). Complete ERA5 from 1940: Fifth generation of ECMWF atmospheric reanalyses of the global climate. *Copernicus Climate Change Service (C3S) Data Store (CDS).*

Hourdin, F., Mauritsen, T., Gettelman, A., Golaz, J. C., Balaji, V., Duan, Q., et al. (2017). The art and science of climate model tuning. *Bulletin of the American Meteorological Society*, *98*(3), 589–602. https://doi.org/10.1175/BAMS-D-15-00135.1

Kay, J. E., Hillman, B. R., Klein, S. A., Zhang, Y., Medeiros, B., Pincus, R., et al. (2012). Exposing global cloud biases in the Community Atmosphere Model (CAM) using satellite observations and their corresponding instrument simulators. *Journal of Climate*, *25*(15), 5190–5207. https://doi.org/10.1175/JCLI-D-11-00469.1

Larson, V. E. (2017). CLUBB-SILHS: A parameterization of subgrid variability in the atmosphere. *arxiv*. Retrieved from http://arxiv.org/abs/1711.03675

Larson, V. E., Domke, S., & Griffin, B. M. (2019). Momentum transport in shallow cumulus clouds and its parameterization by higher-order closure. *Journal of Advances in Modeling Earth Systems*, *11*, 3419–3442. https://doi.org/10.1029/2019MS001743

Lauritzen, P. H., Nair, R. D., Herrington, A. R., Callaghan, P., Goldhaber, S., Dennis, J. M., et al. (2018). NCAR release of CAM-SE in CESM2.0: A reformulation of the spectral element dynamical core in dry-mass vertical coordinates with comprehensive treatment of condensates and energy. *Journal of Advances in Modeling Earth Systems*, *10*(7), 1537–1570. https://doi.org/10.1029/2017MS001257

Lawrence, D. M., Fisher, R. A., Koven, C. D., Oleson, K. W., Swenson, S. C., Bonan, G., et al. (2019). The Community Land Model Version 5: Description of new features, benchmarking, and impact of forcing uncertainty. *Journal of Advances in Modeling Earth Systems*, *11*(12), 4245–4287. https://doi.org/10.1029/2018MS001583

Ma, H. Y., Xie, S., Klein, S. A., Williams, K. D., Boyle, J. S., Bony, S., et al. (2014). On the correspondence between mean forecast errors and climate errors in CMIP5 models. *Journal of Climate*, *27*(4), 1781–1798. https://doi.org/10.1175/JCLI-D-13-00474.1

Mauritsen, T., & Enger, L. (2008). On the use of shear-dependent turbulent length-scales. *Quarterly Journal of the Royal Meteorological Society*, *134*(631), 539–540. https://doi.org/10.1002/qj.218

Morales, A., Posselt, D. J., Morrison, H., & He, F. (2019). Assessing the influence of microphysical and environmental parameter perturbations on orographic precipitation. *Journal of the Atmospheric Sciences*, *76*(5), 1373–1395. https://doi.org/10.1175/JAS-D-18-0301.1

Morris, M. D. (1991). Factorial sampling plans for preliminary computational experiments. *Technometrics*, *33*(2), 161. https://doi.org/10.2307/1269043

Nardi, K. M., Zarzycki, C. M., & Larson, V. E. (2024). Data and code accompanying 'A method for interpreting the role of parameterized turbulence on global metrics in the Community' [Dataset]. *Earth System Model*. https://doi.org/10.26208/SJQR-5M36

Nardi, K. M., Zarzycki, C. M., Larson, V. E., & Bryan, G. H. (2022). Assessing the sensitivity of the tropical cyclone boundary layer to the parameterization of momentum flux in the Community Earth System Model. *Monthly Weather Review*, *150*(4), 883–906. https://doi.org/10.1175/MWR-D

Pathak, R., Sahany, S., & Mishra, S. K. (2020). Uncertainty quantification based cloud parameterization sensitivity analysis in the NCAR Community Atmosphere Model. *Scientific Reports*, *10*(1), 17499. https://doi.org/10.1038/s41598-020-74441-x

Pettett, A., & Zarzycki, C. M. (2023). The 1996 Mid-Atlantic winter flood: Exploring climate risk through a storyline approach. *Journal of Hydrometeorology*, *24*(12), 2259–2280. https://doi.org/10.1175/jhm-d-22-0146.1

Qian, Y., Wan, H., Yang, B., Golaz, J. C., Harrop, B., Hou, Z., et al. (2018). Parametric sensitivity and uncertainty quantification in the version 1 of E3SM atmosphere model based on short perturbed parameter ensemble simulations. *Journal of Geophysical Research: Atmospheres*, *123*(23), 13046–13073. https://doi.org/10.1029/2018JD028927

Qian, Y., Yan, H., Hou, Z., Johannesson, G., Klein, S., Lucas, D., et al. (2015). Parametric sensitivity analysis of precipitation at global and local scales in the Community Atmosphere Model CAM5. *Journal of Advances in Modeling Earth Systems*, *7*(2), 382–411. https://doi.org/10.1002/2014MS000354

Reynolds, R. W., Rayner, N. A., Smith, T. M., Stokes, D. C., & Wang, W. (2002). An improved in situ and satellite SST analysis for climate. *Journal of Climate*, *15*(13), 1609–1625. https://doi.org/10.1175/1520-0442(2002)015<1609:aiisas>2.0.co;2

Simpson, I. R., Bacmeister, J. T., Sandu, I., & Rodwell, M. J. (2018). Why do modeled and observed surface wind stress climatologies differ in the trade wind regions? *Journal of Climate*, *31*(2), 491–513. https://doi.org/10.1175/JCLI-D-17-0255.1

Smalley, M. A., Suselj, K., Lebsock, M. D., & Witte, M. K. (2022). Coupling warm rain with an eddy diffusivity/mass flux parameterization: 2. Sensitivities and comparison to observations. *Journal of Advances in Modeling Earth Systems*, *14*(8). https://doi.org/10.1029/2021MS002729

Stull, R. (1988). An introduction to boundary layer meteorology.

Suselj, K., Posselt, D., Smalley, M., Lebsock, M. D., & Teixeira, J. (2020). A new methodology for observation-based parameterization development. *Monthly Weather Review*, *148*(10), 4159–4184. https://doi.org/10.1175/MWR-D-20-0114.1

Trenberth, K. E., & Fasullo, J. T. (2010). Simulation of present-day and twenty-first-century energy budgets of the southern oceans. *Journal of Climate*, *23*(2), 440–454. https://doi.org/10.1175/2009JCLI3152.1

Vignesh, P. P., Jiang, J. H., Kishore, P., Su, H., Smay, T., Brighton, N., & Velicogna, I. (2020). Assessment of CMIP6 cloud fraction and comparison with satellite observations. *Earth and Space Science*, *7*(2). https://doi.org/10.1029/2019EA000975

Wan, H., Rasch, P. J., Zhang, K., Qian, Y., Yan, H., & Zhao, C. (2014). Short ensembles: An efficient method for discerning climate-relevant sensitivities in atmospheric general circulation models. *Geoscientific Model Development*, *7*(5), 1961–1977. https://doi.org/10.5194/gmd-7-1961-2014

Wehner, M. F., Reed, K. A., Li, F., Prabhat, Bacmeister, J., Chen, C. T., et al. (2014). The effect of horizontal resolution on simulation quality in the Community Atmospheric Model, CAM5.1. *Journal of Advances in Modeling Earth Systems*, *6*(4), 980–997. https://doi.org/10.1002/2013MS000276

Xie, S., Ma, H. Y., Boyle, J. S., Klein, S. A., & Zhang, Y. (2012). On the correspondence between short- and long-time-scale systematic errors in CAM4/CAM5 for the year of tropical convection. *Journal of Climate*, *25*(22), 7937–7955. https://doi.org/10.1175/JCLI-D-12-00134.1

Zarzycki, C. (2023). zarzycki/betacast [Software]. https://doi.org/10.5281/zenodo.8184863

Zarzycki, C. M., & Ullrich, P. A. (2017). Assessing sensitivities in algorithmic detection of tropical cyclones in climate data. *Geophysical Research Letters*, *44*(2), 1141–1149. https://doi.org/10.1002/2016GL071606

Zhang, H., Wang, M., Guo, Z., Zhou, C., Zhou, T., Qian, Y., et al. (2018). Low-cloud feedback in CAM5-CLUBB: Physical mechanisms and parameter sensitivity analysis. *Journal of Advances in Modeling Earth Systems*, *10*(11), 2844–2864. https://doi.org/10.1029/2018MS001423